Post-translational polymodification of 1-tubulin regulates motor protein localisation in platelet production and function

Khan, Abdullah; Slater, Alexandre; Maclachlan, Annabel; Nicolson, Phillip; Pike, Jeremy; Reyat, Jasmeet; Yule, Jack; Stapley, Rachel; Rayes, Julie; Thomas, Steven; Morgan, Neil

DOI:
10.3324/haematol.2020.270793

haematologica
Journal of The Ferrata Storti Foundation

Post-translational polymodification of β1-tubulin regulates motor protein localisation in platelet production and function

by Abdullah O. Khan, Alexandre Slater, Annabel Maclachlan, Phillip L.R. Nicolson, Jeremy A. Pike, Jasmeet S. Reyat, Jack Yule, Rachel Stapley, Julie Rayes, Steven G. Thomas, and Neil V. Morgan

Haematologica 2020 [Epub ahead of print]

Citation: Abdullah O. Khan, Alexandre Slater, Annabel Maclachlan, Phillip L.R. Nicolson, Jeremy A. Pike, Jasmeet S. Reyat, Jack Yule, Rachel Stapley, Julie Rayes, Steven G. Thomas, and Neil V. Morgan. Post-translational polymodification of β1-tubulin regulates motor protein localisation in platelet production and function.
doi:10.3324/haematol.2020.270793

Post-translational polymodification of β1-tubulin regulates motor protein localisation in platelet production and function

Abdullah O. Khan[1*], Alexandre Slater[1], Annabel Maclachlan[1], Phillip L.R. Nicolson[1], Jeremy A. Pike[1,2], Jasmeet S. Reyat[1], Jack Yule[2], Rachel Stapley[1], Julie Rayes[1], Steven G. Thomas[1,2], and Neil V. Morgan[1*]

[1]Institute of Cardiovascular Sciences, College of Medical and Dental Sciences, University of Birmingham, Edgbaston, Birmingham, UK, B15 2TT

[2]Centre of Membrane and Protein and Receptors (COMPARE), University of Birmingham and University of Nottingham, Midlands, UK

*Correspondence: a.khan.4@bham.ac.uk, N.V.Morgan@bham.ac.uk.

Abstract

In specialised cells, the expression of specific tubulin isoforms and their subsequent post-translational modifications drive and coordinate unique morphologies and behaviours. The mechanisms by which β1-tubulin, the platelet and megakaryocyte (MK) lineage restricted tubulin isoform, drives platelet production and function remains poorly understood. We investigated the roles of two key post-translational tubulin polymodifications (polyglutamylation and polyglycylation) on these processes using a cohort of thrombocytopenic patients, human induced pluripotent stem cell (iPSC) derived MKs, and healthy human donor platelets. We find distinct patterns of polymodification in MKs and platelets, mediated by the antagonistic activities of the cell specific expression of Tubulin Tyrosine Ligase Like (TTLLs) and Cytosolic Carboxypeptidase (CCP) enzymes. The resulting microtubule patterning spatially regulates motor proteins to drive proplatelet formation in megakaryocytes, and the cytoskeletal reorganisation required for thrombus formation. This work is the first to show a reversible system of polymodification by which different cell specific functions are achieved.

Introduction

Microtubules are large, cytoskeletal filaments vital to a host of critical functions including cell division, signalling, cargo transport, motility, and function[1,2]. The question of how ubiquitously expressed filaments can facilitate complex and highly unique behaviours (such as neurotransmitter release and retinal organisation) has been addressed by the concept of the tubulin code[3,4]. This paradigm accounts for the specialisation of microtubules and their organisation by describing a mechanism in which particular cells express lineage restricted isoforms of tubulin. These cell specific isoforms are then subject to a series of post-translational modifications (PTMs) which alter the mechanical properties of microtubules, and their capacity to recruit accessory proteins (e.g. motor proteins)[1,2,4,5].

A host of PTMs have been reported in a range of cell types, including tyrosination, acetylation, glutamylation, glycylation, and phosphorylation. The loss of specific tubulin PTMs has been linked to disease and dysfunction in motile and non-motile cilia (including respiratory cilia, retinal cells), spermatogenesis, muscular disorders, and neurological development[1,4,6–11]. Despite an increasing understanding of the importance of tubulin PTMs in disease, the role of the tubulin code in the generation of blood platelets from their progenitors, megakaryocytes (MKs) remains poorly understood.

Platelets are the smallest component of peripheral blood, and circulate as anucleate cells with an archetypal discoid shape maintained by a microtubule marginal band[12,13]. Antagonistic motor proteins maintain the resting state of the marginal band, and during platelet activation a motor dependent mechanism results in sliding which extends the marginal band and causes the transition to a spherical shape[13–15].

Conversely megakaryocytes are the largest and rarest haematopoeitic cell of the bone marrow. These cells are characteristically large, polyploid cells with unique morphological structures (e.g. the invaginated membrane system (IMS)) required to facilitate the production of thousands of blood platelets and packaged within them the required pro-thrombotic factors[15,16]. MKs form long, beaded extensions into the lumen of bone marrow sinusoids - where these proplatelet extensions then experience fission under the flow of sinusoidal blood vessels which results in the release of barbell shaped pre-platelets and platelets into the blood stream[16].

Both MKs and platelets express a lineage-restricted isoform of β1-tubulin encoded by the gene *TUBB1*[17]. In humans, *TUBB1* mutations have been shown to result in impaired platelet production, with a resulting macrothrombocytopenia[18,19]. More recently, a C-terminal truncation of β1**-**tubulin has been shown to cause a macrothrombocytopenia, suggesting that C-terminal modifications may be drivers of protein function and causative of the disease phenotype observed[20].

While the loss of β1-tubulin is known to result in macrothrombocytopenia, the mechanisms by which this isoform of tubulin effects the dramatically different cytoskeletal behaviours of platelets and MKs remains poorly understood. In the context of the tubulin code, MKs and platelets present a particularly interesting model. Both cells express β1**-**tubulin, but undergo markedly different cytoskeletal changes. To date, acetylation and tyrosination have been the PTMs primarily reported in MKs and platelets, however neither modification is specific to the C-terminal tail encoded by *TUBB1*. Fiore *et al.* show that a C-terminal truncation of β1-tubulin phenocopies

the complete loss of the protein[20]. We therefore hypothesise that PTMs specific to the C-terminus of TUBB1 are required for the complex morphological rearrangements required for both MK and platelet function.

The C-terminal tail of β1 tubulin is particularly rich in glutamate residues which are often targeted for two key PTMs implicated in human disease. Polyglutamylation and polyglycylation are PTMs which target glutamate residues on both tubulin subunits (α and β) and result in the addition of glutamate or glycine residues respectively[1,2,21]. As both PTMs target the same residue they are together referred to as polymodification. Polymodification has been observed in microtubules in centrioles, axenomes, neuronal outgrowths, and mitotic spindles[1,2].

To date polyglycylation has not been reported in MKs or platelets. Recently Van Dijk *et al.* reported on the polyglutamylation of β1 tubulin downstream of the integrin $\alpha 2_b \beta_3$ in a CHO cell line engineered to express TUBB1, murine MKs, and platelets spread on fibrinogen[22]. In this work, we report the effects of the loss of the C-terminus of β1-tubulin in patients with rare *TUBB1* variants linked to the low platelet counts. Using induced pluripotent stem cell (iPSC) derived MKs and CRISPR knockout, we report a mechanism of polymodification which distinctly patterns β1-tubulin in MKs and platelets to spatially co-ordinate key motors. We describe the graded, cell specific expression of enzymes which mediate this, and finally report a novel gene, *TTLL10,* which is associated with excessive bleeding.

Methods

Study Approval.

Whole blood was obtained for each experiment from healthy volunteers under the University of Birmingham's ERN 11-0175 license 'The regulation of activation of platelets'. The Genotyping and Phenotyping of Platelets (GAPP) study was approved by the National Research Ethics Service Committee West Midlands – Edgbaston (REC reference 06/MRE07/36). Participants gave written informed consent in compliance with the Declaration of Helsinki. The GAPP study is included in the National Institute for Health Research Non-Malignant Haematology study portfolio (ID 9858), and registered at ISRCTN (http://www.isrctn.org) as ISRCTN77951167.

Whole exome sequencing (WES).

To identify the possible causative variants in these families we sequenced the whole exome of the affected individuals with the SureSelect human All Exon 50 Mb kit (Agilent Technologies) and sequenced on the HiSeq 2500 (Illumina) with 100 bp paired-end reads.

Stem Cell Culture and iPSC MK differentiation.

Gibco human episomal induced pluripotent stem cell line was purchased from Thermo Scientific and cultured on Geltrex basement membrane in StemFlex medium (Thermo Scientific). iPSC differentiation to mature, proplatelet forming megakaryocytes was performed using a protocol based on work published by Feng *et al.*[23] The IDT Alt-R®RNP system was used to target and knock-out TUBB1. iPSC transfection was performed using Lipofectamine Stem (Life Technologies) according to manufacturer instructions.

TUBB1 Homology Modelling.

Homology models of TUBB1 WT and variants were made using SWISS MODEL software[24–27], using the solved TUBB3 heterodimer as a template PDB: 5IJ0[28]. TUBB1 and TUBB3 share approximately 80% sequence identity, and the model created corresponds to residues 1-425 of TUBB1. (Note that the C-terminal tail of TUBB1 is not presented in this model as there is no known or homologous structure available for this highly divergent sequence. The C-terminal portion of this model is used only as a means to visualise the effect of genetic variations on the C-terminal tail of TubB1).

Statistics.

Statistical analysis was performed using GraphPad PRISM 7. Specifics of each test are detailed in the figure legends of the relevant figures. P values below 0.05 were considered significant.

Detailed Materials and Methods can be seen in the Supplementary section.

Results

Identification and initial characterisation of *TUBB1* variants in patients with inherited thrombocytopenia and platelet dysfunction.

Using whole exome sequencing and Congenica Clinical genetic variant interpretation software[29] of patients recruited to the GAPP (Genotyping and Phenotyping of Platelets) study, two C-terminal *TUBB1* variants were identified in unrelated families presenting with macrothrombocytopenia (Figures 1 A, S1). Affected individuals in Family A were found to be heterozygous for an arginine to tryptophan amino acid substitution (c.1075C>T, p.R359W) in *TUBB1*. Individuals in this family also carry a *GFI1B* variant (p.Cys168Phe). Variants in both genes have been linked to thrombocytopenia, however only individuals A:1 and A:3 (carrying *TUBB1* variants), present with a macrothrombocytopenia (107 and 85 x 10^9/L respectively). Individual A:2 carries the *GFI1B* variant but is WT for *TUBB1* and presents with a normal platelet count (221 x 10^9/L). Individuals A:1 and A:3 also present with significantly higher immature platelet fractions (IPFs) and mean platelet volumes (MPVs) when compared to their *TUBB1* WT relatives (53.5% and 55.1% compared to 25.5%, MPV for A:1 and A:3 too large for measurement). This variation in count, IPF and platelet morphology in individuals with the *TUBB1* R359W variant may suggest that the *TUBB1* variant is linked to the macrothrombocytopenia observed.

Family/patient B was an elderly gentleman (now deceased) with a G insertion and subsequent frameshift truncation of the β1-tubulin protein 19 amino acids from the site of insertion (c.1080insG, p.L361Afs*19) [30,31]. This patient had a severe thrombocytopenia with a platelet count of 11 x 10^9/L and an MPV above 13.4 (Figure 1B). At the time of study, IPF measurement was unavailable.

p.L361Afs*19 is absent in the latest version of the gnomad database (accessed October 2020), while p.R359W is a rare variant with a frequency of 6.78 x 10^{-3} (gnomad accessed October 2020) with a significant pathogenicity prediction score of 25.4 using CADD (Combined Annotation Dependent Depletion), where a score of greater or equal to 20 indicates the 1% most deleterious sequence variants in the genome. Both variants were analysed using *in silico* bioinformatic tools and were scored as 'uncertain significance' based on the current ACMG guidelines[32] (Figure S1). Both *TUBB1* variants are positioned towards the C-terminal region of β1-tubulin as indicated in figures 1 C and D. This region is positioned away from the dimer interface with α-tubulin, and the glutamate rich C-terminal tail, not present in the model, is an established site for PTM (Figure 1 C,D)[1]. Both affected *TUBB1* sequence variants are highly conserved in mammals (Figure 1 E). R359 is found within a loop region towards the C-terminus of tubulin, and we predict mutating this residue would not cause dramatic misfolding within the protein secondary structure. R359 does form direct polar contacts with the N-terminal helix and removing this contact through the sequence variant to the hydrophobic tryptophan may result in minor structural changes to the connected C-terminal regions, potentially affecting PTM or interactions with critical microtubule accessory proteins (MAPs) (Figure 1 C, D). Similarly, the G insertion and subsequent frameshift effectively deletes the C-terminus of the protein and would thus, if the protein folds correctly, result in effects similar, or more extreme, to the substitution of R359.

Patient B demonstrated a significant reduction in surface P-selectin expression and fibrinogen binding by flow cytometry in response to all agonists tested (Figure S1). Family A showed no change in the levels of surface receptor expression, but weak P-selectin and fibrinogen responses when activated with a low concentration ADP, CRP, and PAR-1, suggesting a mild functional defect (Figure S1 C,). Patient B also showed marked reduced expression of P-selectin and fibrinogen uptake in response to the same activation agonists (Figure S1 D, E). Patients with C-terminal variants in this study and others previously reported by Fiore *et al.* present with a macrothrombocytopenia also found in individuals with a complete loss of the β1-tubulin, suggesting that the C-terminal tail is likely critical to the function of TUBB1 in the roles of microtubules in MKs and platelets[18–20]. As this C-terminal tail is rich in glutamate residues which are often targeted for polymodification, we began to investigate the polymodification of β1-tubulin.

C-terminal variants of β1-tubulin fold correctly and demonstrate a reduction in polymodification.

First, we investigated the effects of the two patient variants (p.R359W and p.L361Afs*19) on the folding and potential polymodification of β1 tubulin. We designed, generated, and validated a β1 tubulin-mApple fusion construct (Figure S2). This plasmid was further mutated to harbour each of the patient variants (p.R359W and p.L361Afs*19), and an artificial C-terminal truncation which specifically deletes the glutamate rich C-terminal tail (Figures S2, 2A). The WT β1 tubulin construct was transfected into Hek293T cells and co-stained for polyglutamylated and polyglycylated tubulin specifically. Transfected cells are exclusively positive for both residues indicating that β1 tubulin is indeed polymodified (Figure 2B). Expression of each of the mutated constructs show that both patient variants and the C-terminal truncation fold correctly (Figure 2C). Furthermore each of the results in a consistent and significant reduction in polymodification (Figure 2D). This data indicates that both patient variants result in a correctly folded β1 tubulin which has a similar effect to a truncation of the C-terminus, and is further supported by western blotting of mutant constructs (Figure S3) which show a significant reduction in polymodification.

iPSC-derived proplatelet forming MKs are both polyglycylated and polyglutamylated.

The tubulin code posits that a highly lineage and species specific expression of modifying enzymes mediates cell specific PTMs. While our transfection data successfully indicates that β1-tubulin is indeed polymodified, and that each of our patient genetic variants result in the expression of a functional β1-tubulin with a C-terminal truncation, data from both human MKs and platelets is needed to dissect the role of polymodification in these cells.

To date, polyglycylation has not been reported in either platelets or megakaryocytes. Polyglutamylation has recently been reported in a modified CHO cell line and human platelets. To investigate polymodification in human megakaryocytes, we adapted a directed differentiation protocol previously reported by Feng *et al.* to generate large populations of mature, proplatelet forming cells (Figure S4). iPSC-MK were stained for CD42b as a marker for mature, and hence TUBB1 expressing, MKs, and both polyglutamylated and polyglycylated tubulin. CD42b+ cells were found to be positive for both polyglutamylated tubulin and polyglycylated tubulin (Figure 3A), while neighbouring cells in the sample negative for CD42b did not demonstrate these polymodifications (Figure 3B).

Across multiple differentiations we consistently yielded a purity of ~50-60% CD42b+ cells (Figure 3C), which on analysis are positive for both polyglutamylated and polyglycylated tubulin (Figure 3D). Finally, 100% of proplatelet forming cells observed across replicates were positive for both polymodifications (Figure 3E), and this was further confirmed by western blot (Figure 3F).

CRISPR knockout of β1-tubulin results in a complete loss of proplatelet formation.

To date, the loss of TUBB1 has not been studied in human MKs. We generated an iPSC line with a CRISPR mediated bi-allelic loss of function mutation in the N-terminus of the coding region of TUBB1 (Figure 3G, S5). The mutation of the TUBB1 start codon on both alleles results in a complete loss of expression (absence of T2 band in Figure 3H) and proplatelet formation in vitro (Figure 3I, J – right panel). Unfortunately, our attempts to generate C-terminal truncations through CRISPR in iPSC-MKs were unsuccessful as multiple guides targeting the 3' end of the TUBB1 gene failed to cleave the genomic sequence. Interestingly while TUBB1 knock-out clones stain positively for polyglutamylated and polyglycylated tubulin, the distribution of these residues is disturbed when compared to WT platelet forming iPSC-MKs (Figure 3K). While polyglycylated and polyglutamylated residues form a distinct peripheral band around WT MKs as shown in figure 3K, the knockout cells demonstrate a diffuse tubulin staining (evidenced by line profiles in Figure S7). Figure 3L shows quantification of this staining whereby wildtype iPSC-Mks display higher mean intensity than knockout constructs in polyglycylated tubulin, however no significant quantitative change in polyglutamylation was observed. This is the first data demonstrating the effects of the loss of TUBB1 expression in human MKs.

Platelets demonstrate a different pattern of polymodification.

We hypothesised that the β1-tubulin polymodifications evident in MKs might be differently regulated between resting and activated platelets. We therefore compared immunofluorescence staining of polyglutamylated and polyglycylated tubulin between resting platelets and cells spread on fibrinogen and collagen.

Resting platelets demonstrate polyglutamylated tubulin which partially colocalises with the β1-tubulin marginal band unlike MKs which demonstrate extensive polyglycylation in proplatelet forming cells (Figure 4A). On fibrinogen and collagen spreading, polyglutamylation is evident, notably at the marginal band of spreading cells on fibrinogen (Figure 4B). A lack of polyglycylation is consistent in both resting and activated platelets. Western blotting of resting platelets and cells activated through stimulation by CRP over time does not show an increase in the total amount of polyglutamylated tubulin (Figure 4C). An increase in the co-localisation between β1-tubulin and polyglutamylated residues suggests that while the total polyglutamylation of platelets remains unchanged through activation, the distribution of these residues is altered (Figure 4D). We confirmed the polyglutamylation (and loss of polyglycylation) in microthrombi generated by CRP stimulation (Figure 4E, F, G). This data shows that while polyglutamylation and re evident in platelet producing iPSC-MKs, polyglycylation is completely lost in mature platelets. This is the first evidence of a system whereby these competitive polymodifications are dramatically altered between the 'parent' and terminal cell, suggesting markedly different roles for these residues in mediating the function and activity of β1 tubulin. Acetylation and tyrosination have been previously reported in

platelets, however their role in maintaining the marginal band and/or driving morphological change on platelet activation remains unclear[13]. To determine whether the polyglutamylation of the marginal band we observe thus far coincides with these PTMs, we performed a time course of spreading on fibrinogen to determine whether there is an equivalent increase in either acetylation or tyrosination of the marginal band. Interestingly, we find a significant decrease in acetylation and tyrosination over time (between 0 and 10 minutes), while a notable polyglutamylation of the marginal band is evident from the earliest time point (10 minutes spreading on fibrinogen) and does not decrease (Figure 4F,G).

Platelet and MK polymodifications regulate motor protein localisation to drive both proplatelet formation and platelet shape change on activation.

Polyglutamylation has been reported as a means by which motor protein processivity is regulated, and like in neuronal cells, MK proplatelet formation is known to be driven by a mechanism of dynein mediated proplatelet sliding[33]. Similarly, the antagonistic movement of dynein and kinesin are known to maintain the marginal band in resting platelets[13].

To test if polymodification affects the spatial distribution of motors, we performed a time course of platelet spreading on fibrinogen and measured co-localisation between polyglutamylated tubulin and dynein (DNAL1 - axonemal light chain 1). We observe a loss of co-localisation between dynein and polyglutamylated residues upon platelet spreading (Figure 5A, B). Interestingly, axonemal dynein is also localised towards the leading edge of spread platelets (Figure 5A). This data suggests that the increased polyglutamylation of the marginal band observed on platelet spreading drives an outward movement of axonemal dynein. To investigate the role of axonemal dynein specifically in this process, we also stained spreading platelets for cytoplasmic dynein and observe a central distribution, suggesting an alternative role for cytoplasmic dynein in platelets (Figure S6).

The loss of co-localisation between polyglutamylated tubulin and dynein was confirmed on both collagen and fibrinogen spread platelets (5C, E). This spatial relationship was also observed between polyglutamylated tubulin and kinesin-1, a motor protein recently reported to be important in platelet secretion on platelet spreading (Figure 5 D, F)[34].

This data suggests that polyglutamylated tubulin is involved in localising motor proteins during platelet activation and spreading. The actions of kinesin and dynein are known to be critical to driving platelet shape change on activation, and this work is consistent with previous reports of polyglutamylated tubulin altering the processivity of motors in axons.

We then investigated the role of these polymodifications on the distribution of motors in iPSC-MKs. In proplatelet extensions axonemal dynein and kinesin-1 are both evident along the length of the proplatelet shaft (Figure 5G). β1-tubulin knockout cells show no proplatelet formation, and a significant reduction in the co-localisation of dynein with polyglutamyulated residues when compared to WT iPSC-MKs (Figure 5H,I). No significant change in the colocalisation of these residues with kinesin-1 is observed between WT and knockout iPSC-MKs (Figure 5J).

MK and platelet polymodification is regulated through the expression of both modifying and reversing enzymes.

We hypothesise that the expression of cell specific subsets of effecting (TTLL) and reversing (CCP) enzymes are required to achieve the distinctive polymodification we observe in MKs and platelets. We designed a qRT-PCR panel to interrogate the expression of the 13 known mammalian TTLLs and 6 CCPs. We generated RNA from iPSC-MKs at different stages of maturation (Figures 6A, S4A). Day 1 (d1) cells are representative of a pool of haematopoeitic stem cells (HSCs) and MK progenitors, while day 5 (d5) cells are comprised of 60% CD41/42b+ cells (Figures 6A , S4 E). Finally, day 5 cells treated with heparin to induce proplatelet formation (d5 + Hep) were used to interrogate whether there is any specific up-regulation of TTLLs and/or CCPs on proplatelet formation (Figures 6A, S4D).

GAPDH housekeeping controls for each of the 3 samples (d1, d5, d5+Hep) show equivalent amplification of the housekeeping control, while results for TTLL family proteins show a number of enzymes expressed at different levels across the maturation of these cells (Figure 6B,C). Candidate TTLLs observed in the initial endpoint PCR were taken forward for quantification across replicates generated from multiple differentiations (Figure 6C, D). We find a significantly increased expression of TTLL1, TTLL2, TTLL4, and TTLL10 on proplatelet formation in cells treated with heparin (** $p = 0.0081$, * $p = 0.0105$, * $p = 0.0260$, *** $p = 0.0004$ respectively) (Figure 6D). CCP family enzymes were also found to be expressed in maturing MKs, notably CCP1, 3, 4, 5, and 6 (Figure 6E), with CCP4 and 6 up-regulated on proplatelet production (* $p = 0.0130$, *** $p = 0.0009$) (Figure 6F).

To investigate TTLL and CCP expression in platelets, we repeated this panel on RNA extracted from resting and CRP stimulated donor platelets. We found that none of the TTLLs and CCPs observed in iPSC MKs were consistently expressed across donors with the exception of TTLL7, a known polyglutamylase (Figure 6I, complete gel in figure S10)[35]. No differences between resting and activated platelets were observed (Figure 6I). This data shows a markedly different pattern of TTLL and CCP expression in both MKs and platelets, correlating with the observed differences in polymodification.

***TTLL10* variants maybe associated with moderate to severe bleeding in 3 unrelated families.**

Our qRT-PCR screen reveals that a number of TTLL and CCPs are up-regulated during the process of platelet production, including the polyglycylase TTLL10. Whole exome sequencing data from patients recruited to the GAPP study identified 3 unrelated families with rare and novel variants in the *TTLL10* gene (Figure 6J, figure S12, 13). Extensive *in silico* analysis was undertaken on the *TTLL10* variants which were predicted as 'uncertain significance' using current ACMG guidelines (Figure S12, 13)[32]. Two of the three variants result in frameshifts towards the N-terminus of the protein, preceding the ATP binding region (p.Pro15Argfs*38 (novel) and p.Val249Glyfs*57 (frequency 2.15×10^{-3}) (Figure 6J). The final family has a missense p.Arg340Trp variant ($3.34 \times 10^{\neq 5}$ frequency).

All three families report normal platelet counts, aggregation and secretion, and present an established history of moderate to severe bleeding, including cutaneous bruising and menorrhagia (Figure 6K). Family A demonstrated a consistently high MPV (normal ranges Mean Platelet Volume (fL) (7.83-10.5), while families B and C do not.

Interestingly, one of the patients (A 1:1) was re-recruited, and on platelet spreading on fibrinogen coated coverslips we observed a marked increase in platelet area compared to controls when imaged using widefield and single molecule localisation microscopy (SMLM) (Figure 6L).

Discussion

We hypothesised that a system of polymodification (polyglutamylation and polyglycylation) targeting the glutamate rich C-terminus of β1 tubulin isoform and analogous to similar PTMs demonstrated in cilia and neuronal cells, is a likely mechanism by which the interactions of β1 tubulin with key motors are regulated in both MKs and platelets.

We report that mature and proplatelet forming CD42b+ iPSC-MKs demonstrate both polyglutamylation and polyglycylation (polymodification). We observe a markedly different distribution of these PTMs in the resting platelet, where polyglycylation is lost and polyglutamylation is partially co-localised to the marginal band. On platelet activation, we observe a marked change in the localisation of polyglutamylation specific to the marginal band. In iPSC-MKs with a CRISPR knockout of TUBB1, we see a complete loss of proplatelet formation and lose the distinct reorganisation of polyglutamylated and polyglycylated tubulin around the periphery of MKs as seen in WT cells.

MK proplatelet extensions are known to be driven by a system of dynein mediated microtubule sliding, while the marginal band in a resting platelet has been shown to be maintained by the antagonistic movement of dynein and kinesin[13,14,36]. Interestingly, polyglutamylation has been reported as a mechanism of altering motor protein processivity, with in vitro assays suggesting that polyglutamylation of β1 tubulin isoforms like TUBB1 and TUBB3 accelerates these motors[28]. We show a significant effect of polyglutamylation on the spatial localisation of dynein and kinesin, supporting in vitro assays which suggest that polyglutamylation is an accelerator of motor proteins.

We report two unrelated patient families with rare *TUBB1* C-terminal variants (an R359W missense and a L361Afs*19 frameshift linked to macrothrombocytopenia). Interestingly within family A, a second genetic variant in the *GFI1B* gene, which directly affects the TUBB1 promoter is observed. Individuals within family A positive for the GFI1B variant but WT for TUBB1 have normal platelet counts and a milder increase in MPV and IPF, indicating that the macrothrombocytopenia within the family is possibly linked to the TUBB1 variant, but suggesting a potential additive role for the *GFI1B* variant which is a focus for future study. Both the clinical phenotype and laboratory investigations points to variable expressivity of the 2 genetic variants contributing to the overall phenotypes observed.

We go on to show through the expression of these variants in Hek293T cells that each variant results in a dysfunctional β1 tubulin protein which is most likely to mirror the effects of a C-terminal truncation.

The system of polymodification evidenced in iPSC-MKs is analogous to the PTM of ciliated cells, and so we reasoned that axonemal dynein, an isoform of the motor exclusive to axonemes, may play a role in both platelet formation and activation[6,37,38]. We find evidence of axonemal dynein on both proplatelet extensions and at the leading edge of spreading platelets. To our knowledge this is the first evidence of a functional role of axonemal dynein outside of classical ciliated structures. In our TUBB1 knockout MKs, we observe a decrease in the colocalisation of dynein to polyglutamyulated tubulin, suggesting that the loss of proplatelet formation observed in these cells is due to a dysregulation of the dynein-mediated microtubule sliding known to drive the elongation of the proplatelet shaft[39]. The similarlities between flagella and MK proplatelet extensions have been discussed

previously, Italiano et al. observe structures similar to flagella in taxol treated MKs, an idea which led to the microtubule telescoping experiment reported by Patel et al. and Italiano et al. [39,40].

Our data suggests a tightly regulated, reversible system of polymodification which must be mediated by the cell specific expression of TTLLs and CCPs. Our expression profiles show a number of TTLLs and CCPs are expressed by MKs, while only the polyglutamylase TTLL7 is expressed by platelets consistent with the different patterns of polymodification oberved in these cells. In MKs we find expression of two TTLLs known to be involved in glycylation - the initiase TTLL3 and the elongase TTLL10, with a significant increase in the expression of TTLL10 on platelet production. Our findings support a role of TTLL10 as a polyglycylase on co-expression with TTLL3 as reported by Ikegami et al. in cell lines through co-transfection experiments. Finally, we report a novel gene, TTLL10, in three unrelated families with excessive bleeding.

We identify 3 unrelated families with TTLL10 variants which result in an increase in an established history of bleeding which provides an invaluable insight to the potential role of polyglycylation in the context of platelet production and function. Our data shows that both TTLL3 and TTLL10 are expressed in platelet producing MKs. Our patient cohort do not lose TTLL3 function, and as such the action of TTLL3 as an initiase will occupy glutamate residues which would otherwise be polyglutamylated. In these patients we likely see a loss of polyglycylation, but no coincident increase in polyglutamylation due to the normal function of the initiase (TTLL3). As polyglutamylation and monoglycylation are unaffected, platelet counts (and production) are normal, however, affected individuals appear to have an increased platelet volume and bleeding, suggesting a role for the extended glycine tail in regulating platelet size, with a downstream effect on the ability of platelets to prevent bleeding.

Patel et al. describe a system by which continuous polymerisation is key to the dynein mediated sliding required for platelet production[39]. This work, alongside reports of tyrosination, acetylation, and polyglutamylation in different MK models, suggests that tubulin PTMs are likely part of a highly dynamic system in which polymerising microtubules are subject to modifications which coordinate platelet production and packaging. Future work will interrogate the interplay between different PTMs, and how they fit into a highly dynamic landscape of MT polymerisation and function. Indeed, in our KO TUBB1 cells we do not observe a complete loss of polymodification, suggesting that compensatory mechanisms which target other isoforms of tubulin may come into play. There is likely a more extensive effect on the expression of tubulins and their interplay with other cytoskeletal proteins which should be a focus of future work. Similarly, the role of these PTMs will need to be further validated in primary human CD34 derived MKs.

This work supports the paradigm of a 'tubulin code' and the importance of microtubule patterning in healthy, and thus diseased, MKs and platelets. We provide novel insights into the mechanisms by which β1 tubulin functions in these unique cells.

Author Contributions. AOK and NVM devised and performed experiments. AOK and NVM wrote the manuscript. AS performed homology modelling, cloning, transfection, and platelet spreading experiments. AM performed platelet spreading and analysis of patient sequencing data. PLR performed platelet preparations and reviewed the manuscript. JAP developed and applied image analysis workflows. JSR assisted with western blotting. JY contributed to platelet preparations. SGT, JR, RS and NVM reviewed the manuscript.

ACKNOWLEDGEMENTS

We thank the families for providing samples and our clinical and laboratory colleagues for their help. This work was supported by the British Heart Foundation (PG/13/36/30275; FS/13/70/30521; FS/15/18/31317; PG/16/103/32650; IG/18/2/33544). The authors would like to thank the TechHub and COMPARE Core facilities at the University of Birmingham. AOK is a Wellcome funded Sir Henry Wellcome Fellow (218649/Z/19/Z). We thank Professor Steve Watson for his ongoing support and invaluable mentorship.

The authors do not have any conflict of interest.

References

1. Wade RH. On and around microtubules: an overview. Mol Biotechnol. 2009;43(2):177-191.
2. Gadadhar S, Dadi H, Bodakuntla S, et al. Tubulin glycylation controls primary cilia length. J Cell Biol. 2017; 216(9):2701-2713.
3. Ludueña RF. A hypothesis on the origin and evolution of tubulin. Int Rev Cell Mol Biol. 2013;302:41-185.
4. Magiera Maria M, Singh Puja, Janke Carsten. SnapShot: Functions of Tubulin Posttranslational Modifications. Cell. 2018;173(6):1552-1552.e1.
5. Gadadhar S, Bodakuntla S, Natarajan K, Janke C. The tubulin code at a glance. J Cell Sci. 2017;130(8):1347-1353.
6. Wloga D, Joachimiak E, Louka P, Gaertig J. Posttranslational Modifications of Tubulin and Cilia. Cold Spring Harb Perspect Biol. 2017;9(6):a028159.
7. Reiter JF, Leroux MR. Genes and molecular pathways underpinning ciliopathies. Nat Rev Mol Cell Biol. 2017;18(9):533-547.
8. Bosch Grau Montserrat, Masson Christel, Gadadhar Sudarshan, et al. Alterations in the balance of tubulin glycylation and glutamylation in photoreceptors leads to retinal degeneration. J Cell Sci. 2017;130(5):938-949.
9. Ikegami K, Sato S, Nakamura K, Ostrowski LE, Setou M. Tubulin polyglutamylation is essential for airway ciliary function through the regulation of beating asymmetry. Proc Natl Acad Sci U S A. 2010;107(23):10490-10495.
10. Wu HY, Wei P, Morgan JI. Role of Cytosolic Carboxypeptidase 5 in Neuronal Survival and Spermatogenesis. Sci Rep. 2017;7:41428.
11. Vogel P, Hansen G, Fontenot G, Read R. Tubulin tyrosine ligase-like 1 deficiency results in chronic rhinosinusitis and abnormal development of spermatid flagella in mice. Vet Pathol. 2010;47(4):703-712.
12. Dmitrieff S, Alsina A, Mathur A, Nédélec FJ. Balance of microtubule stiffness and cortical tension determines the size of blood cells with marginal band across species. Proc Natl Acad Sci U S A. 2017;114(17):4418-4423.
13. Diagouraga B, Grichine A, Fertin A, Wang J, Khochbin S, Sadoul K. Motor-driven marginal band coiling promotes cell shape change during platelet activation. J Cell Biol. 2014;204(2):177-185.
14. Sadoul K. New explanations for old observations: marginal band coiling during platelet activation. J Thromb Haemost. 2015;13(3):333-346.
15. Poulter Natalie S, Thomas SG. Cytoskeletal regulation of platelet formation: Coordination of F-actin and microtubules. Int J Biochem Cell Biol. 2015;66:69-74.
16. Machlus KR, Italiano JE. The incredible journey: From megakaryocyte development to platelet formation. J Cell Biol. 2013;201(6):785-796.
17. Schwer HD, Lecine P, Tiwari S, Italiano JE, Hartwig JH, Shivdasani RA. A lineage-restricted and divergent beta-tubulin isoform is essential for the biogenesis, structure and function of blood platelets. Curr Biol. 2001;11(8):579-586.
18. Kunishima S, Kobayashi R, Itoh Tomohiko J, Hamaguchi Mo, Saito H. Mutation of the beta1-tubulin gene associated with congenital macrothrombocytopenia affecting microtubule assembly. Blood. 2009;113(2):458-461.
19. Kunishima S, Nishimura S, Suzuki H, Imaizumi M, Saito H. TUBB1 mutation disrupting microtubule assembly impairs proplatelet formation and results in congenital macrothrombocytopenia. Eur J Haematol. 2014;92(4):276-282.
20. Fiore M, Goulas C, Pillois X. A new mutation in TUBB1 associated with thrombocytopenia confirms that C-terminal part of b1-tubulin plays a role in microtubule assembly. Clin Genet. 2017;91(6):924-926.
21. Natarajan K, Gadadhar S, Souphron J, Magiera MM, Janke Carsten. Molecular interactions between tubulin tails and glutamylases reveal determinants of glutamylation patterns. EMBO Rep. 2017;18(6):1013-1026.
22. Dijk J, Bompard G, Cau J, et al. Microtubule polyglutamylation and acetylation drive microtubule dynamics critical for platelet formation. BMC Biol. 2018;16(1):116.
23. Feng Q, Shabrani N, Thon JN, et al. Scalable generation of universal platelets from human induced pluripotent stem cells. Stem Cell Rep. 2014;3(5):817-831.
24. Waterhouse Andrew, Bertoni Martino, Bienert Stefan, et al. SWISS-MODEL: homology modelling of protein structures and complexes. Nucleic Acids Res. 2018;46(W1):W296-W303.
25. Bienert S, Waterhouse A, Beer TAP, et al. The SWISS-MODEL Repository—new features and functionality. Nucleic Acids Res. 2016;45(D1):D313-D319.
26. Guex N, Peitsch MC, Schwede T. Automated comparative protein structure modeling with SWISS-MODEL and Swiss-PdbViewer: A historical perspective. Electrophoresis. 2009;30:S162-S173.
27. Benkert P, Biasini M, Schwede T. Toward the estimation of the absolute quality of individual protein structure models. Bioinformatics. 2010;27(3):343-350.

28. Ti SC, Pamula MC, Howes SC, et al. Mutations in Human Tubulin Proximal to the Kinesin-Binding Site Alter Dynamic Instability at Microtubule Plus- and Minus-Ends. Dev Cell. 2016;37(1):72-84.
29. Almazni I, Stapley RJ, Khan AO, Morgan NV. A comprehensive bioinformatic analysis of 126 patients with an inherited platelet disorder to identify both sequence and copy number genetic variants. Hum Mutat. 2020;41(11):1848-1865.
30. Johnson B, Lowe GC, Futterer J, et al. Whole exome sequencing identifies genetic variants in inherited thrombocytopenia with secondary qualitative function defects. Haematologica. 2016;101(10):1170-1179.
31. Khan AO, Stapley R, Pike JA, et al. Novel gene variants in patients with platelet-based bleeding using combined exome sequencing and RNAseq murine expression data. J Thromb Haemost. 2020 Oct 6. [Epub ahead of print]
32. Richards S, Aziz N, Bale S, et al. Standards and guidelines for the interpretation of sequence variants: a joint consensus recommendation of the American College of Medical Genetics and Genomics and the Association for Molecular Pathology. Genet Med. 2015;17(5):405-424.
33. Bender M, Thon JN, Ehrlicher AJ, et al. Microtubule sliding drives proplatelet elongation and is dependent on cytoplasmic dynein. Blood. 2015;125(5):860-868.
34. Adam F, Kauskot A, Kurowska M, et al. Kinesin-1 Is a New Actor Involved in Platelet Secretion and Thrombus Stability. Arterioscler Thromb Vasc Biol. 2018;38(5):1037-1051.
35. Ikegami K, Mukai M, Tsuchida J, Heier RL, Macgregor GR, Setou M. TTLL7 is a mammalian beta-tubulin polyglutamylase required for growth of MAP2-positive neurites. J Biol Chem. 2006;281(41):30707-30716.
36. Sirajuddin M, Rice LM, Vale RD. Regulation of microtubule motors by tubulin isotypes and post-translational modifications. Nat Cell Biol. 2014;16(4):335-344.
37. O'Hagan R, Silva M, Nguyen Ken CQ, et al. Glutamylation Regulates Transport, Specializes Function, and Sculpts the Structure of Cilia. Curr Biol. 2017;27(22):3430-3441.
38. Wloga D, Dave D, Meagley J, Rogowski K, Jerka-Dziadosz M, Gaertig J. Hyperglutamylation of tubulin can either stabilize or destabilize microtubules in the same cell. Eukaryot Cell. 2010;9(1):184-193.
39. Patel R, Richardson Jennifer L, Schulze Harald, et al. Differential roles of microtubule assembly and sliding in proplatelet formation by megakaryocytes. Blood. 2005;106(13):4076-4085.
40. Italiano JE, Lecine P, Shivdasani R A, Hartwig J H. Blood platelets are assembled principally at the ends of proplatelet processes produced by differentiated megakaryocytes. J Cell Biol. 1999;147(6):1299-1312.
41. Kremers G, Hazelwood KL, Murphy CS, Davidson MW, Piston DW. Photoconversion in orange and red fluorescent proteins. Nat Methods. 2009;6(5):355-358.
42. Khan AO, Simms VA, Pike JA, Thomas SG, Morgan NV. CRISPR-Cas9 Mediated Labelling Allows for Single Molecule Imaging and Resolution. Sci Rep. 2017;7(1):8450.
43. Khan AO, White CW, Pike JA, et al. Optimised insert design for improved single-molecule imaging and quantification through CRISPR-Cas9 mediated knock-in. Sci Rep. 2019;9(1):14219.
44. Smith CW, Raslan Z, Parfitt L, et al. TREM-like transcript 1: a more sensitive marker of platelet activation than P-selectin in humans and mice. Blood Adv. 2018;2(16):2072-2078.
45. Pike JA, Simms VA, Smith CW, et al. An adaptable analysis workflow for characterization of platelet spreading and morphology. Platelets. 2020:1-5.
46. Berthold MR, Cebron N, Dill F, et al. KNIME-the konstanz information miner: version 2.0 and beyond. AcM SIGKDD explorations Newsletter. 2009;11:26-31.
47. Sommer C, Strahle C, Kothe F, A. Hamptrecht F. ilastik: Interactive Learning and Segmentation Toolkit. In: Eighth IEEE International Symposium on Biomedical Imaging (ISBI). Proceedings. 2011;230-233.
48. Khan AO, Maclachlan A, Lowe GC, et al. High-throughput platelet spreading analysis: a tool for the diagnosis of platelet-based bleeding disorders. Haematologica. 2020;105(3):e124-e128.
49. McDonald JH, Dunn KW. Statistical tests for measures of colocalization in biological microscopy. J Microsc. 2013;252(3):295-302.

Figure Legends

Figure 1. Candidate *TUBB1* variants and their hypothesised effect on the C-terminus of β1-tubulin. (A, B) Two unrelated families were identified as carrying genetic variations in the *TUBB1* gene within 6 base pairs of one another. The first, family A, is comprised of 3 individuals, two of whom carry an Arginine to Tryptophan (p.R359W) coding variant. Interestingly, all 3 individuals in family A harbour an additional *GFI1B* variant. However, the individuals with the reported *TUBB1* variant (A:1 and A:3) present with a macrothrombocytopenia and high IPF, while the patient without the R359W *TUBB1* variant presented with a normal platelet count. The second family is comprised of a single individual, recently deceased, with a frameshift variant 6 base pairs from the missense change reported in family A. In this individual's case, the insertion of a guanine nucleotide results in a frameshift with a premature stop codon 19 amino acids from the leucine to alanine change. Platelet count normal range 147 - 327 x 10^9/L, (n = 40), MPV normal range 7.8 - 12.69 fL (n = 40), IPF normal range 1.3 - 10.8% (n = 40). (C) The C-terminal tail is downstream of both genetic variants in these families, and projects away from the dimer:dimer interface. The C-terminal sequence of TUBB1 is rich in glutamate residues which can be targeted for polymodification. (D) Based on homology modelling of TUBB1, we predict that the missense variant reported in family A is likely to affect the fold of the C-terminal tail, while the frameshift causes a truncation of this region. (Black arrows indicating the position of the R359 residue). (E) The arginine residue substitution in family A is highly conserved across species, as are sequences adjacent to the frameshift in patient B.

Figure 2. Cells expressing WT and mutated β1-tubulin demonstrate C-terminal polymodification. (A) Constructs carrying WT, patient variants (p.R359W and p.L361Afs*19), and a C-terminal tail truncation of β1-tubulin fused to the fluorescent reporter mApple at the N-terminus were designed and cloned. (B) The WT construct was first transfected into Hek293T cells, which were then fixed and immunostained for polyglutamylated and polyglycylated tubulin residues specifically. (C,D) A comparison of the WT and mutated constructs show a reduction in polyglutamylation and polyglycylation in each mutant when compared to the WT. (n = 3 independent differentiations, S.D. plotted on graphs. 2-way ANOVA with multiple comparisons performed to establish significance.)

Figure 3. Mature, proplatelet forming iPSC-MKs are both polyglutamylated and polyglycylated. TubB1 knockout iPSC-MKs do not form proplatelets and demonstrate disordered polymodified tubulin. (A) iPSC-MKs co-stained for CD42 and polyglycylated or polyglutamylated tubulin show that these cells are positive for both polymodifications. Both polyglutamylated and polyglycylated tubulin are evident in proplatelet extensions, including nascent platelet swellings on the proplatelet shaft. (B) Neighbouring CD42b- cells are negative for both polymodifications (indicated by red arrows). (C,D) Approximately 50-60% of cells in multiple differentiations are CD42b+, and these cells are 100% double positive for polymodification and CD42b+. (E) All proplatelet extensions observed are positive for polymodification. (F) Polyglutamylation and polyglycylation are evident by western blotting in mature iPSC-MKs derived from 3 separate differentiations. (G) iPSC were transfected with a TUBB1 targeting guide RNA, after which indel positive cells were isolated and sequenced to positively identify a bi-allelic insertion-deletion mutant (clone T2). (H) This clone was further analyzed and loss of β1-tubulin expression was confirmed by qRT-PCR. (I,J) A comparison of proplatelet production in wild-type vs. TUBB1 KO cells revealed a complete loss of proplatelet formation in mutant CD41/42b+ cells. (K) TUBB1 knock-out clones show a disordered arrangement of polymodified residues when compared to WT cells. KO cells do not demonstrate the re-organisation of tubulin to the periphery of the cell evident in WT iPSC-MKs (indicated by red arrows). (L) A measure of the polyglutamylation and polyglycylation in WT vs. KO clones reveals a significant increase

in polyglycylation in mutant cells consistent with an aberrant accumulation of these residues. (n = 3 independent differentiations, S.D. plotted on graphs)

Figure 4. Platelet activation results in polyglutamylation of the marginal band (A) Resting platelets show a partial polyglutamylation of the marginal band and a loss of the polyglycylation evident in iPSC-MKs. (B) Platelet spreading on fibrinogen and collagen shows an accumulation of polyglutamylation at the marginal band as platelets spread, and no evidence of polyglycylation. (C) Western blotting of resting and CRP activated platelets confirms the presence of polyglutamylated tubulin and a loss of polyglyclation. No increase in polyglutamylation is evident over time. (D) A measurement of co-localisation (corrected Manders coefficient) between polyglutamylated tubulin and β1-tubulin in resting and spread platelets shows a significant increase in the co-localisation of these modified tubulin residues on platelet activation and spreading. (E) Platelets activated in vitro using CRP were fixed and co-stained for β1-tubulin and polyglutamylated residues, and then imaged in 3D using AiryScan confocal (stacks colourized in Z as indicated by the colour chart in this figure). In these micro-thrombi, polyglutamylation of the marginal band is evident, while polyglycylation is not observed. (F) A time course was performed to compare polyglutamylated tubulin with two other previously reported PTMs in platelets (acetylation and tyrosination). Polyglutamylation is maintained over time, while acetylation and tyrosination decrease significantly as platelets spread. (G) The mean fluorescence intensity of polyglutamylated tubulin is markedly higher than either acetylated or tyrosinated tubulin. (n = 3, S.D., Two-Way ANOVA with multiple comparisons. 10 μm scale bar.)

Figure 5. Polyglutamylation regulates spatial distribution of motor proteins in platelets and MKs. (A, B) Quantification of the co-localisation of dynein, as measured by the corrected Manders coefficient, with polyglutamylated tubulin over time shows a marked decrease in co-localisation between these polymodified residues and the motor over time. (C) In fibrinogen and collagen spread cells, dynein is observed on the periphery of the spread cells, (D) while kinesin-1 is evident as a diffuse punctate stain. (E) Dynein co-localisation with polyglutamylated residues decreases dramatically on platelet spreading in both fibrinogen and collagen (** p = 0.0082 and p = *** 0.0004 respectively). (F) a loss of co-localisation with polyglutamylated tubulin is evident in fibrinogen and collagen spread cells (** p = 0.0017, **** p < 0.0001 respectively). (G) Immunofluorescence staining of iPSC-MKs for polymodified tubulin, dynein, and kinesin-1 show the distribution of both motors along the length of the proplatelet shaft in WT cells. (H, I) In β1-tubulin knock-out iPSC-MKs, no proplatelet extensions are formed and a significant reduction in the co-localisation of dynein to polyglutamlated residues is observed (* p = 0.0166 and * p = 0.0293 respectively), (J) with no significant change in the co-localisation of kinesin-1 with polyglycylated tubulin. (n = 3, S.D., Two-Way ANOVA with multiple comparisons.)

(G) Figure 6. iPSC-MKs and platelets differentially express TTLL and CCP enzymes to regulate polymodifications during MK maturation and platelet production. The loss of TTLL10 is possibly linked to a bleeding phenotype in unrelated human patients. (A) RNA was generated from iPSC-MKs at different stages of terminal differentiation. Day 1 (d1) day 5 (d5) day 5 cells treated with heparin to induce proplatelet formation (d5 + Hep) were used to determine whether an upregulation of these enzymes is evident on platelet production. (B) Samples were amplified with housekeeping GAPDH primers (C) A number of TTLL family enzymes were observed, including TTLLs1, 2, 3, 4, 5, 6, 7, 10, and 13. Of these, a number appeared to be up-regulated in mature and proplatelet forming cells. (D, E) These samples were taken forward and expression was quantified over multiple differentiations using the $\Delta\Delta$CT method TTLL 1, 2, 4, and 10 expression was found to be significantly upregulated on treatment with heparin (** p = 0.0081, * p = 0.0105, * p = 0.0260, *** p = 0.0004 respectively). (F, G, H) A similar panel was performed on CCP enzymes which

reverse polymodifications, with expression of CCP1, 3, 4, 5, and 6 was observed. Statistically significant upregulation of CCPs 4, and 6 were observed on proplatelet production (* p = 0.0130, *** p = 0.0009). (I) In resting (-) and CRP activated (+) platelets from 3 healthy donors TTLL7 was the only modifying enzyme found to be consistently expressed. (J) Three unrelated families were identified within the GAPP cohort, two with frameshift truncations and one with a missense substitution (p.Pro15Argfs*38, p.Val249Glyfs*57, and p.Arg340Trp respectively). (K) All three families present with normal platelet counts and function, but demonstrate an elevated mean platelet volume (MPV) and consistent histories of bleeding including cutaneous bruising and menorrhagia. (L) Patient A:1:1 was recalled and demonstrated abnormally large platelets on spreading on fibrinogen when imaged by widefield and single molecule localisation microscopy (tubulin staining, 10 μm scale bar, 5 μm in cropped image). (n = 3, S.D., Two-Way ANOVA with multiple comparisons performed. Complete unedited gels found in figures S9, S10.)

Figure 7. A system of competitive polymodification of TUBB1 driven by the expression of TTLL and CCP enzymes is required for platelet production and function. We observe a system by which as iPSC-MKs mature and express TUBB1, they acquire both polyglutamylated and polyglycylated tubulin which co-incides with an increase in the expression of glutamylating and glycylating TTLLs and reversing CCPs. A resting platelet is partially polyglutamylated, and on activation the marginal band is further polyglutamylated to drive shape change and spreading through the action of TTLL7. We show that this polymodification spatially affects the position of key motor proteins.

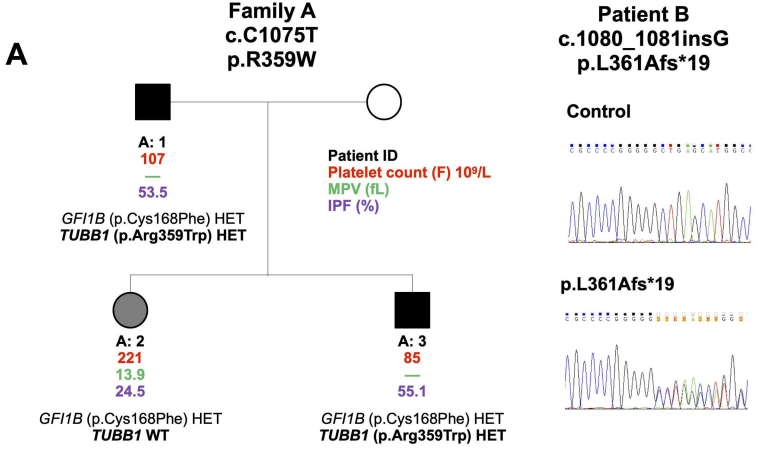

B

Patient	Age	Gender	*TUBB1* Mutation	*GFI1B* Mutation	Plat. count (x10⁹/l)	MPV (fL)	IPF (%)	Secondary defect
A: 1	66	M	p.R359W	p.C168F	107	large	53.5	Yes
A: 2	41	F	WT	p.C168F	221	13.9	24.5	Yes
A: 3	29	M	p.R359W	p.C168F	85	large	55.1	Yes
B:1	*Dec.*	M	p.L361Afs*19	None	11	13.4+	N/A	Yes

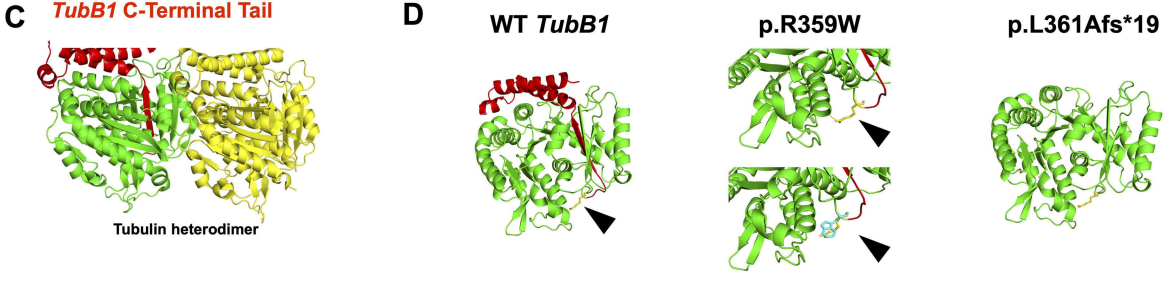

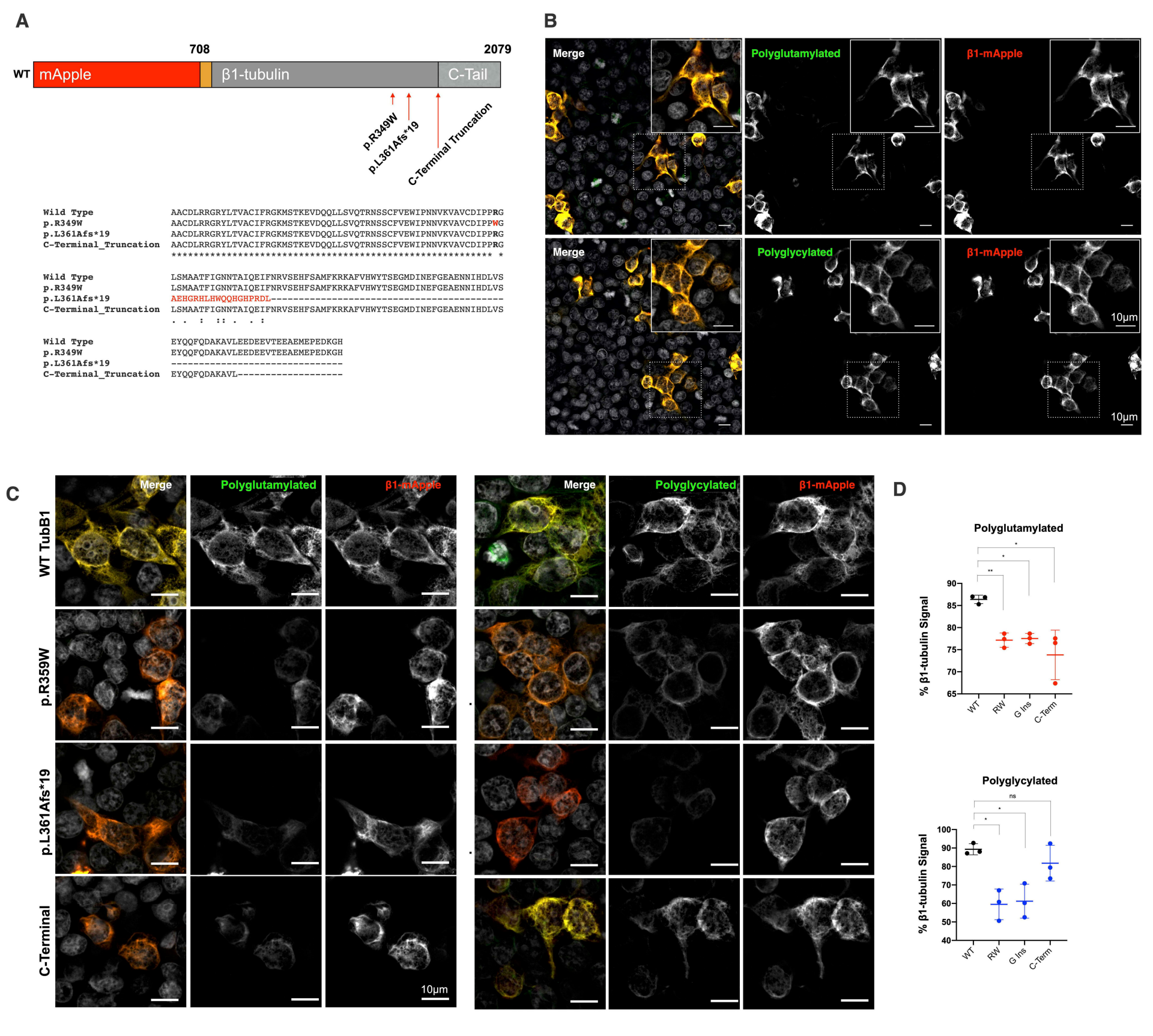
A
708
2079
WT
mApple
β1-tubulin
C-Tail
p.R349W
p.L361Afs*19
C-Terminal Truncation
Wild Type AACDLRRGRYLTVACIFRGKMSTKEVDQQLLSVQTRNSSCFVEWIPNNVKVAVCDIPPRG
p.R349W AACDLRRGRYLTVACIFRGKMSTKEVDQQLLSVQTRNSSCFVEWIPNNVKVAVCDIPPWG
p.L361Afs*19 AACDLRRGRYLTVACIFRGKMSTKEVDQQLLSVQTRNSSCFVEWIPNNVKVAVCDIPPRG
C-Terminal_Truncation AACDLRRGRYLTVACIFRGKMSTKEVDQQLLSVQTRNSSCFVEWIPNNVKVAVCDIPPRG
Wild Type LSMAATFIGNNTAIQEIFNRVSEHFSAMFKRKAFVHWYTSEGMDINEFGEAENNIHDLVS
p.R349W LSMAATFIGNNTAIQEIFNRVSEHFSAMFKRKAFVHWYTSEGMDINEFGEAENNIHDLVS
p.L361Afs*19 AEHGRHLHWQQHGHPRDL
C-Terminal_Truncation LSMAATFIGNNTAIQEIFNRVSEHFSAMFKRKAFVHWYTSEGMDINEFGEAENNIHDLVS
Wild Type EYQQFQDAKAVLEEDEEVTEEAEMEPEDKGH
p.R349W EYQQFQDAKAVLEEDEEVTEEAEMEPEDKGH
p.L361Afs*19
C-Terminal_Truncation EYQQFQDAKAVL
B
Merge
Polyglutamylated
β1-mApple
Merge
Polyglycylated
β1-mApple
10μm
10μm
C
Merge
Polyglutamylated
β1-mApple
Merge
Polyglycylated
β1-mApple
WT TubB1
p.R359W
p.L361Afs*19
C-Terminal
10μm
D
Polyglutamylated
% β1-tubulin Signal
90
85
80
75
70
65
WT
RW
G Ins
C-Term
Polyglycylated
% β1-tubulin Signal
100
90
80
70
60
50
40
ns
WT
RW
G Ins
C-Term

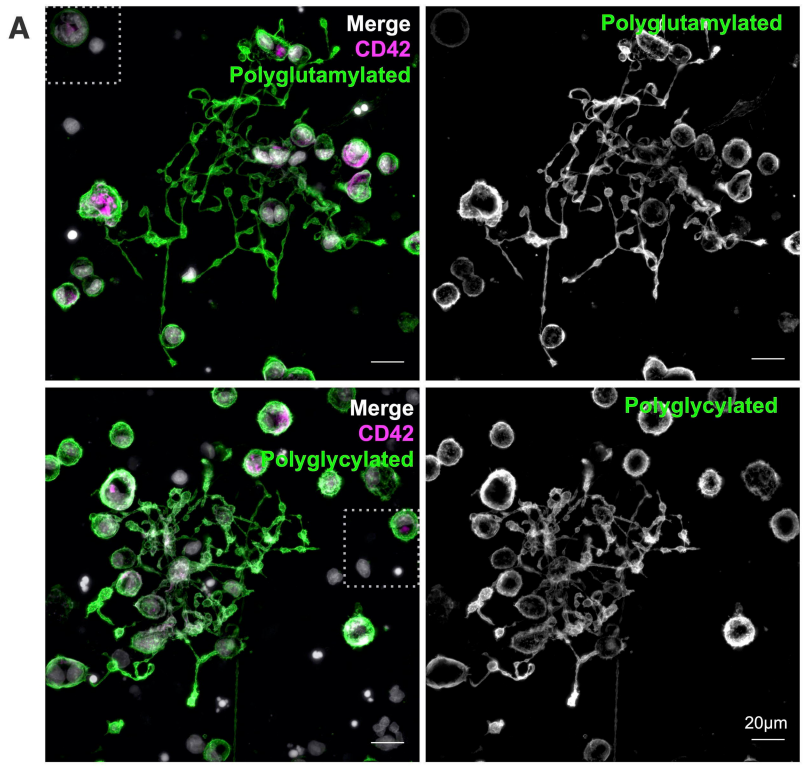
A
Merge
CD42
Polyglutamylated
Polyglutamylated
Merge
CD42
Polyglycylated
Polyglycylated
20μm

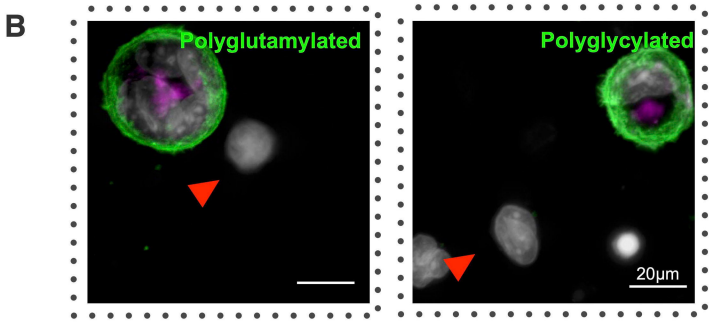
B
Polyglutamylated
Polyglycylated
20μm

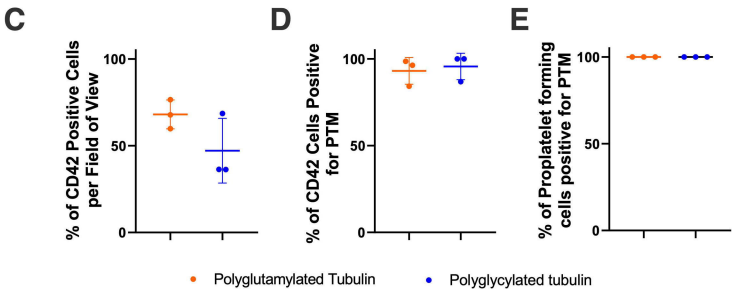
C
% of CD42 Positive Cells per Field of View
D
% of CD42 Cells Positive for PTM
E
% of Proplatelet forming cells positive for PTM
Polyglutamylated Tubulin
Polyglycylated tubulin

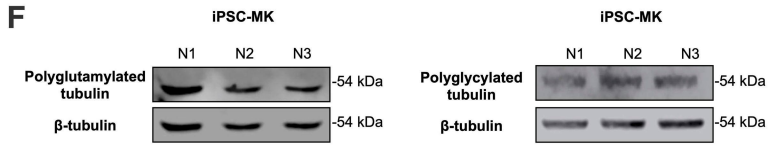
F
iPSC-MK
N1
N2
N3
Polyglutamylated tubulin
-54 kDa
β-tubulin
-54 kDa
iPSC-MK
N1
N2
N3
Polyglycylated tubulin
-54 kDa
β-tubulin
-54 kDa

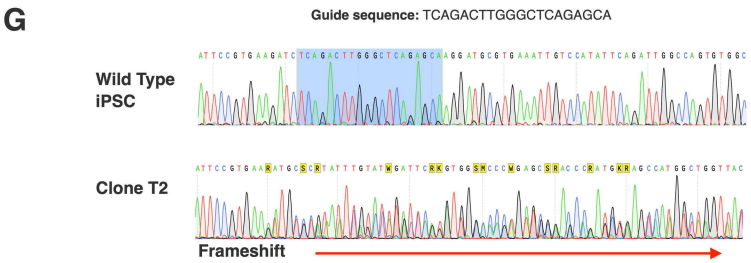
G
Guide sequence: TCAGACTTGGGCTCAGAGCA
Wild Type iPSC
Clone T2
Frameshift

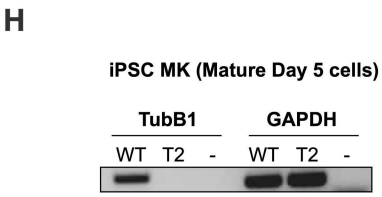
H
iPSC MK (Mature Day 5 cells)
TubB1
GAPDH
WT
T2
-
WT
T2
-

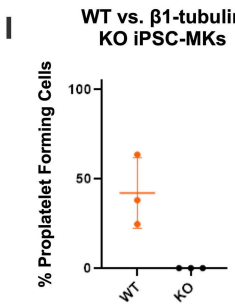
I
WT vs. β1-tubulin KO iPSC-MKs
% Proplatelet Forming Cells
WT
KO

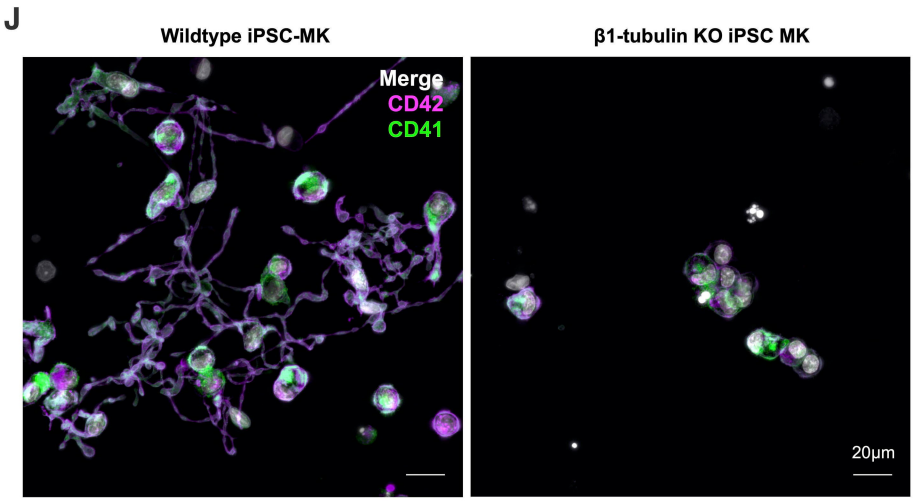
J
Wildtype iPSC-MK
β1-tubulin KO iPSC MK
Merge
CD42
CD41
20μm

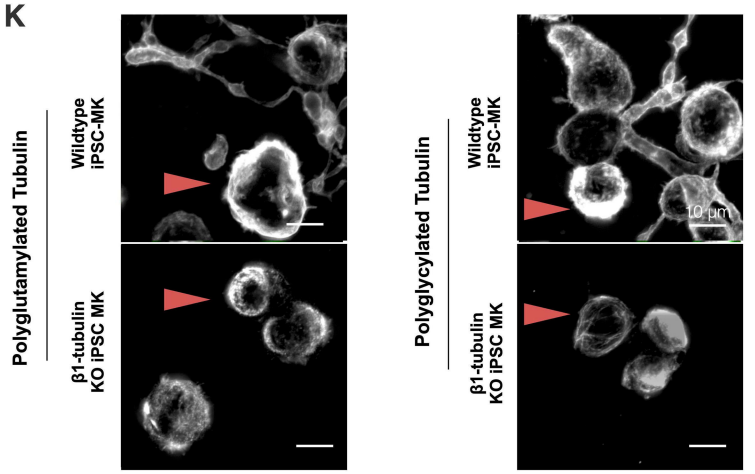
K
Polyglutamylated Tubulin
Wildtype iPSC-MK
β1-tubulin KO iPSC MK
Polyglycylated Tubulin
Wildtype iPSC-MK
β1-tubulin KO iPSC MK
10 μm

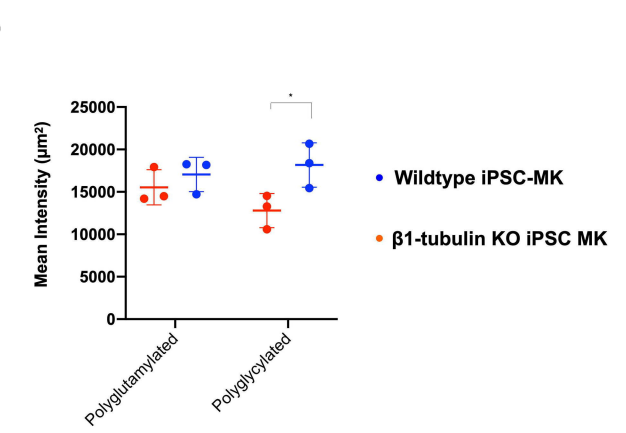
L
Mean Intensity (μm²)
Polyglutamylated
Polyglycylated
Wildtype iPSC-MK
β1-tubulin KO iPSC MK

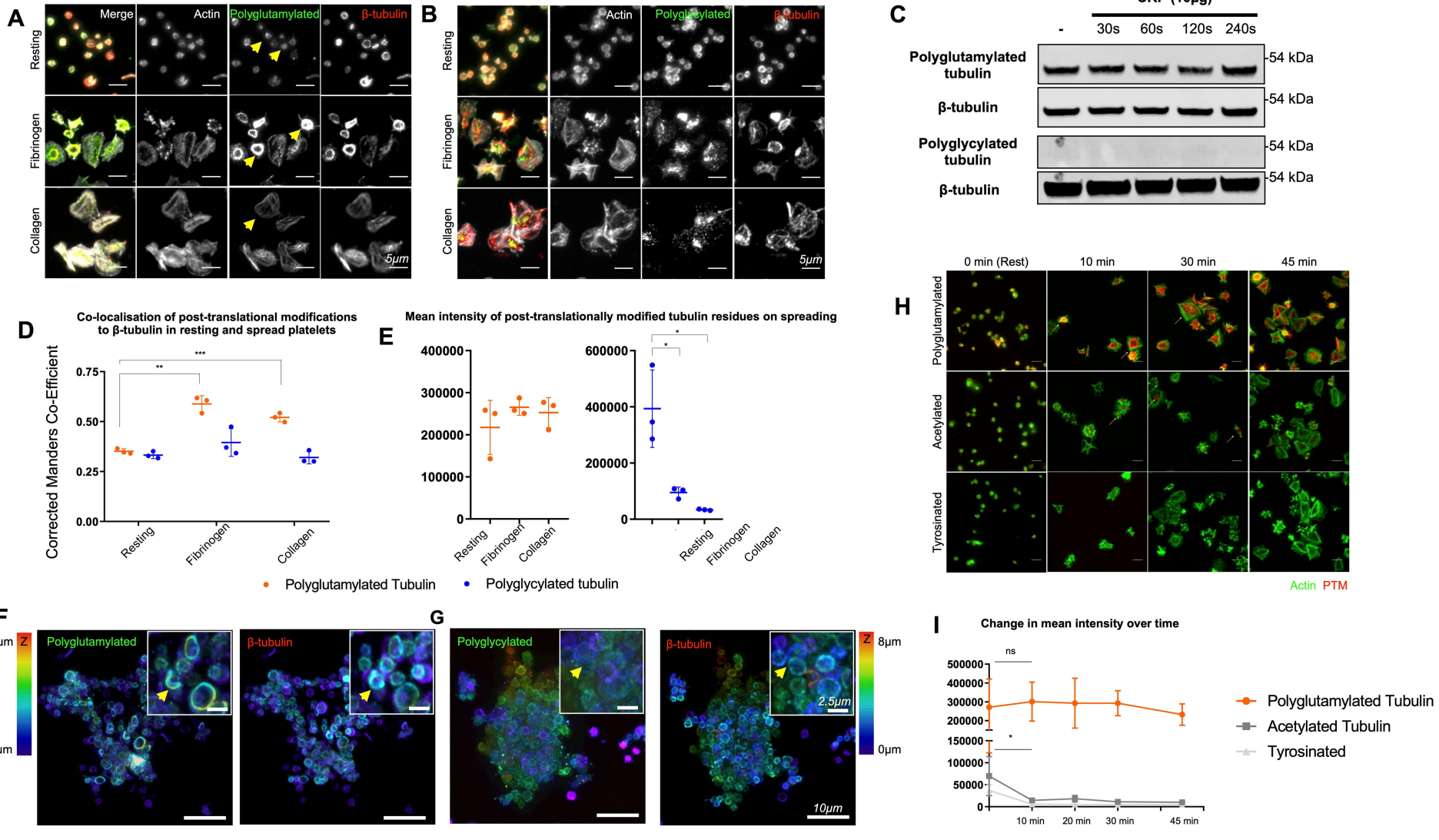
A
Merge
Actin
Polyglutamylated
β-tubulin
Resting
Fibrinogen
Collagen
5μm
B
Actin
Polyglycylated
β-tubulin
Resting
Fibrinogen
Collagen
5μm
C
CRP (10μg)
-
30s
60s
120s
240s
Polyglutamylated tubulin
β-tubulin
Polyglycylated tubulin
β-tubulin
54 kDa
54 kDa
54 kDa
54 kDa
D
Co-localisation of post-translational modifications to β-tubulin in resting and spread platelets
Corrected Manders Co-Efficient
0.75
0.50
0.25
0.00
**
***
Resting
Fibrinogen
Collagen
E
Mean intensity of post-translationally modified tubulin residues on spreading
400000
300000
200000
100000
0
600000
400000
200000
0
*
*
Resting
Fibrinogen
Collagen
Resting
Fibrinogen
Collagen
Polyglutamylated Tubulin
Polyglycylated tubulin
H
0 min (Rest)
10 min
30 min
45 min
Polyglutamylated
Acetylated
Tyrosinated
Actin PTM
F
4.62μm
Z
0μm
Polyglutamylated
β-tubulin
G
Polyglycylated
β-tubulin
2.5μm
10μm
Z
8μm
0μm
I
Change in mean intensity over time
ns
*
500000
400000
300000
200000
150000
100000
50000
0
10 min
20 min
30 min
45 min
Polyglutamylated Tubulin
Acetylated Tubulin
Tyrosinated

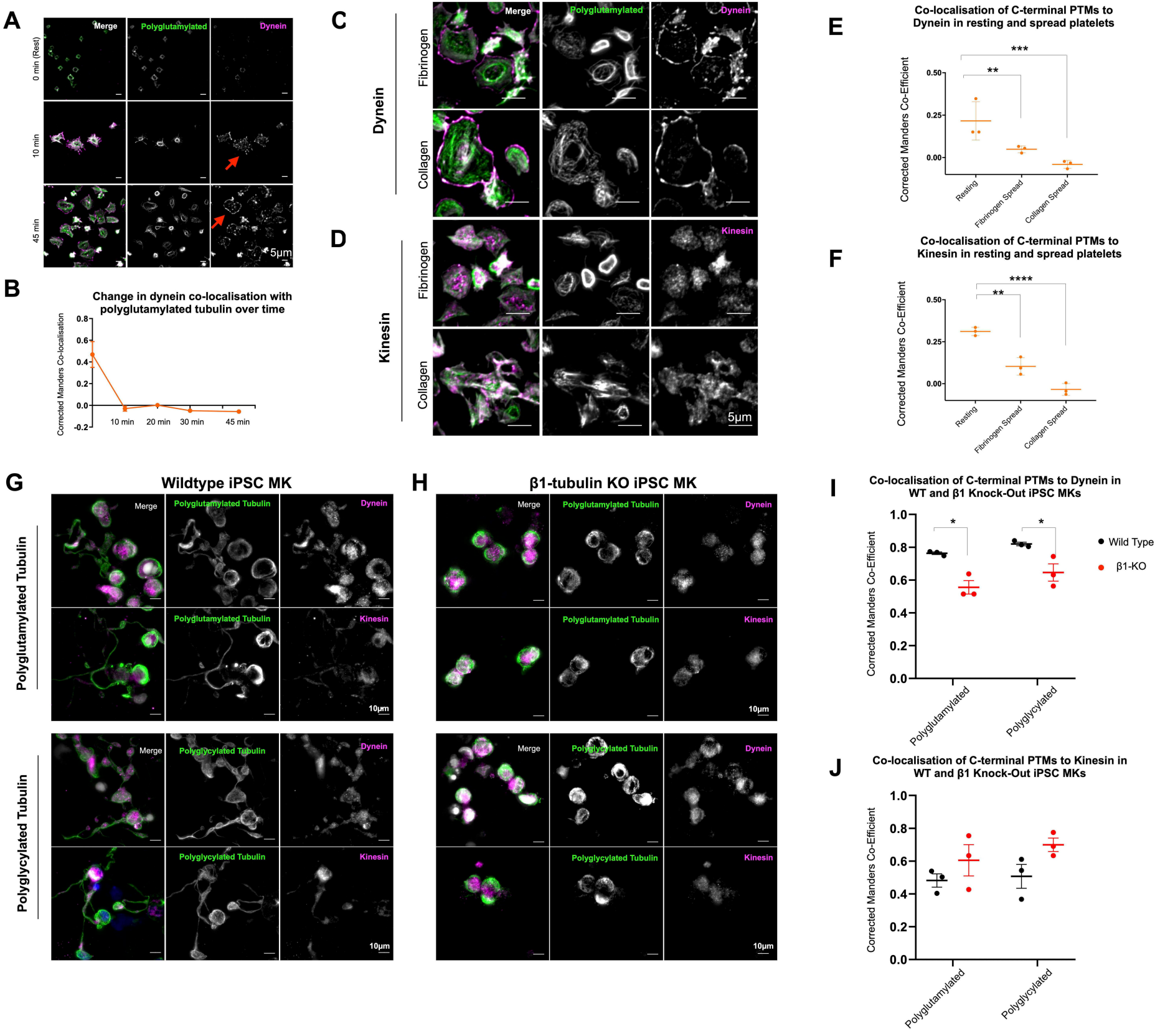
A
Merge
Polyglutamylated
Dynein
0 min (Rest)
10 min
45 min
5µm
B
Change in dynein co-localisation with polyglutamylated tubulin over time
Corrected Manders Co-localisation
0.8
0.6
0.4
0.2
0.0
-0.2
10 min
20 min
30 min
45 min
C
Dynein
Fibrinogen
Collagen
Merge
Polyglutamylated
Dynein
D
Kinesin
Fibrinogen
Collagen
Kinesin
5µm
E
Co-localisation of C-terminal PTMs to Dynein in resting and spread platelets
Corrected Manders Co-Efficient
0.50
0.25
0.00
***
**
Resting
Fibrinogen Spread
Collagen Spread
F
Co-localisation of C-terminal PTMs to Kinesin in resting and spread platelets
Corrected Manders Co-Efficient
0.50
0.25
0.00
****
**
Resting
Fibrinogen Spread
Collagen Spread
G
Wildtype iPSC MK
Polyglutamylated Tubulin
Polyglycylated Tubulin
Merge
Polyglutamylated Tubulin
Polyglycylated Tubulin
Dynein
Kinesin
10µm
H
β1-tubulin KO iPSC MK
Merge
Polyglutamylated Tubulin
Polyglycylated Tubulin
Dynein
Kinesin
10µm
I
Co-localisation of C-terminal PTMs to Dynein in WT and β1 Knock-Out iPSC MKs
Corrected Manders Co-Efficient
1.0
0.8
0.6
0.4
0.2
0.0
*
*
Wild Type
β1-KO
Polyglutamylated
Polyglycylated
J
Co-localisation of C-terminal PTMs to Kinesin in WT and β1 Knock-Out iPSC MKs
Corrected Manders Co-Efficient
1.0
0.8
0.6
0.4
0.2
0.0
Polyglutamylated
Polyglycylated

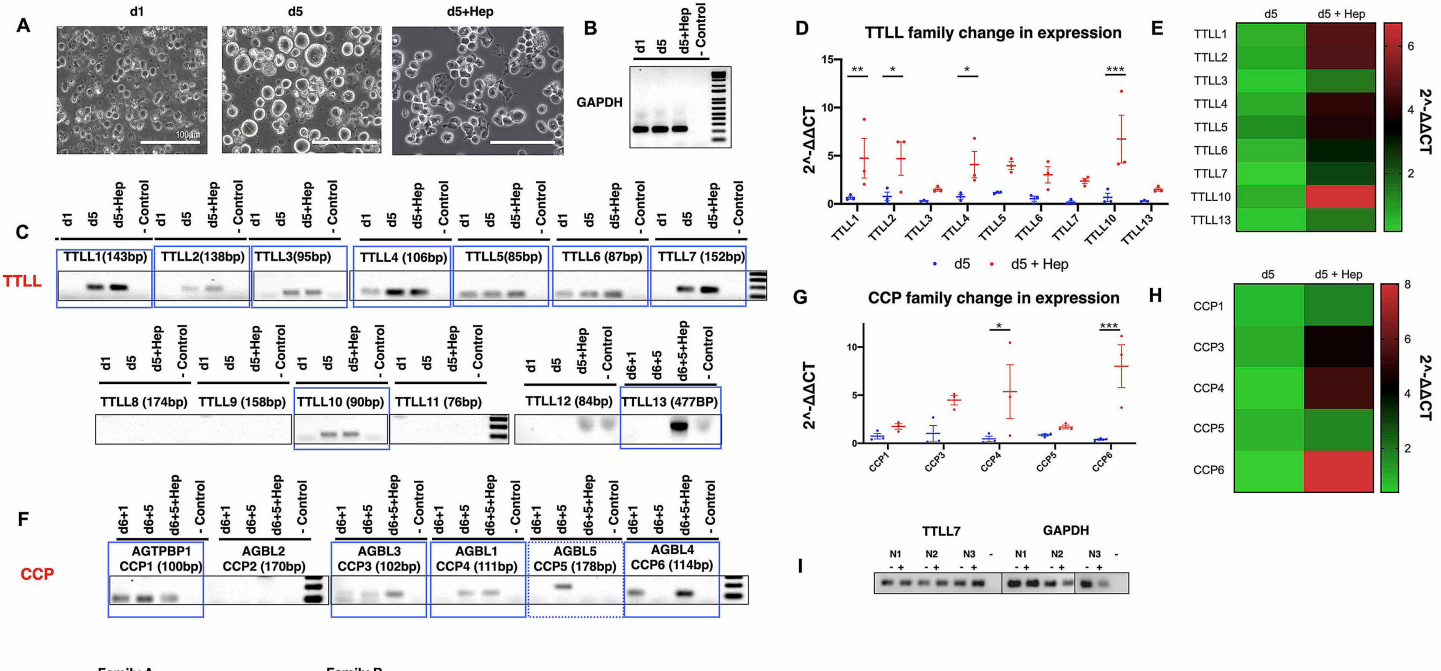

K

Individual	A	Sex	*TTLL10* Variant	Protein effect	Platelet count (x10⁹/l)	IPF	MPV (fL)	Bleeding Phenotype	Functional Defect
A: I:1	34 '84	M	c.462delG	p.Pro155Argfs*38	196	9	12.6	Unreported	Normal aggregometry, secretion.
A: I:2	31		WT		259	7.6	11.7	Menorrhagia	Normal aggregometry, secretion.
A: II:2	11 (2006)	F	c.462delG	p.Pro155Argfs*38	246	4.2	11.3	Epistaxis, easy bruising and prolonged bleeding from minor wounds, required	Normal aggregometry, secretion.
A: II:3	10 (2008)	F	c.462delG	p.Pro155Argfs*38	329	5.6	12.1	Cutaneous bruising, easy bleeding	Normal aggregometry, secretion.
B: II:2	Deceased	F	c.745_746insG	p.Val249Glyfs*57	n/a	n/a	8.6	Easy bruising, menorrhagia	Normal aggregometry, secretion.
B: III:1	29	M	c.745_746insG	p.Val249Glyfs*57	n/a	n/a	9.4	Easy bruising, menorrhagia, bled from tooth extraction.	Normal aggregometry, secretion.
C: III:1	41	F	c.1018C>T	p.Arg340Trp	n/a	n/a	8.0	Cutaneous bruising, Menorrhagia, post partum haemorrhage x 2, bled following	Normal aggregometry, secretion.

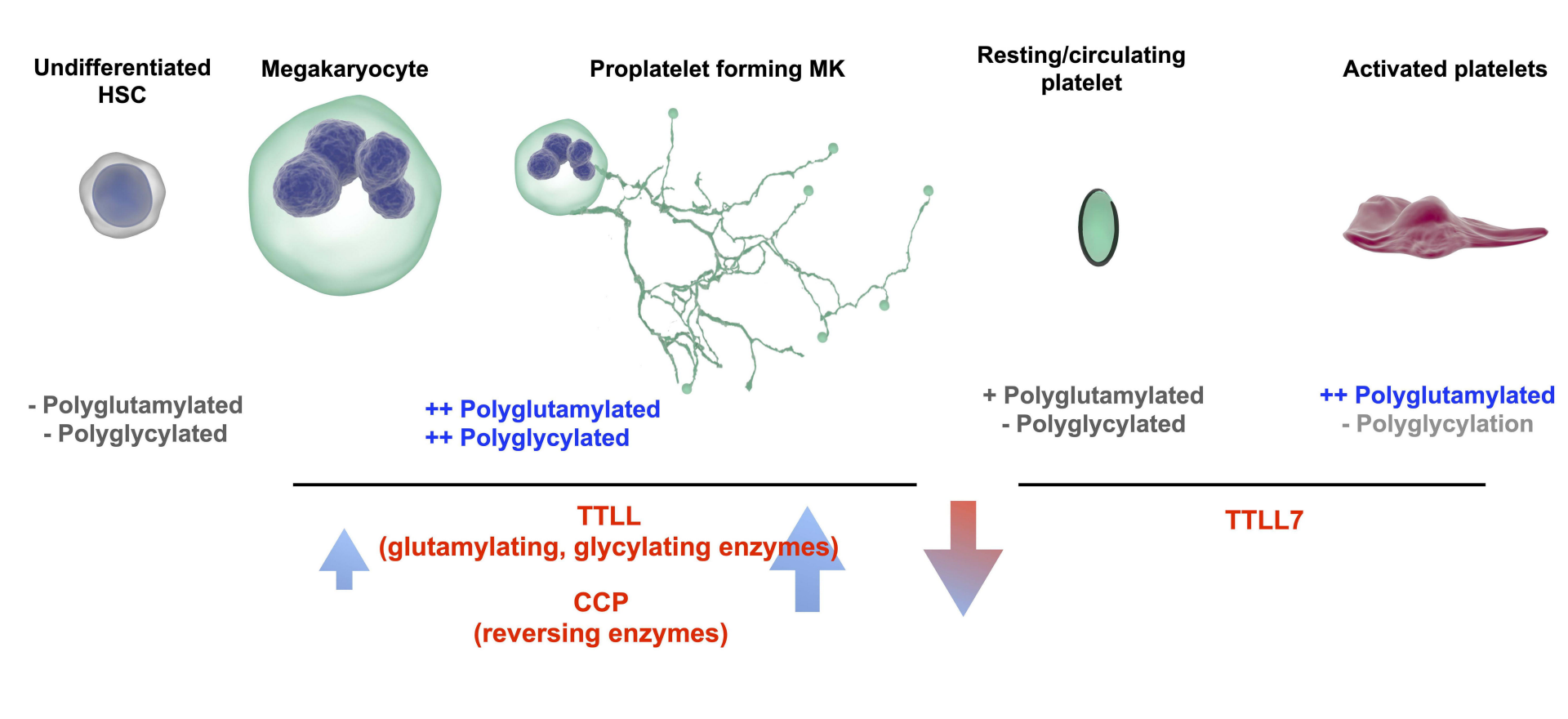
Undifferentiated HSC
Megakaryocyte
Proplatelet forming MK
Resting/circulating platelet
Activated platelets
- Polyglutamylated
- Polyglycylated
++ Polyglutamylated
++ Polyglycylated
+ Polyglutamylated
- Polyglycylated
++ Polyglutamylated
- Polyglycylation
TTLL
(glutamylating, glycylating enzymes)
CCP
(reversing enzymes)
TTLL7

Post-translational polymodification of β1 tubulin regulates motor protein localisation in platelet production and function

Abdullah O. Khan[1]✉, Alexandre Slater[1], Annabel Maclachlan[1], Phillip L.R. Nicolson[1], Jeremy A. Pike[1,2], Jasmeet S. Reyat[1], Jack Yule[2], Rachel Stapley[1], Julie Rayes[1], Steven G. Thomas[1,2], and Neil V. Morgan[1]✉

[1]Institute of Cardiovascular Sciences, College of Medical and Dental Sciences, University of Birmingham, Edgbaston, Birmingham, UK, B15 2TT
[2]Centre of Membrane and Protein and Receptors (COMPARE), University of Birmingham and University of Nottingham, Midlands, UK

Supplementary Materials and Methods

Whole exome sequencing (WES).

To identify the causative mutation in these families we sequenced the whole exome of the affected individuals with the SureSelect human AllExon 50 Mb kit (Agilent Technologies) and sequenced on the HiSeq 2500 (Illumina) with 100 bp paired-end reads. The sequences were aligned to the reference genome (hg19 build), with Novoalign (Novocraft Technologies Sdn Bhd). Duplicate reads, resulting from PCR clonality or optical duplicates, and reads mapping to multiple locations were excluded from downstream analysis. Depth and breadth of sequence coverage was calculated with custom scripts and the BedTools package. Single nucleotide substitutions and small insertion deletions were identified and quality filtered within the SamTools software package and in-house software tools. All calls with a read coverage <4 and a phred-scaled SNP quality of <20 were filtered out. Genetic variants were annotated with respect to genes and transcripts with the Annovar tool. Candidate variants were prioritised according to their frequency in the latest population databases where a rare variant was defined as <0.01.

Platelet preparation.

25 mL volumes of blood were drawn from volunteers into sodium citrate. PRP (platelet-rich plasma) was generated by centrifugation of samples for 20 minutes at 200 g. PRP was further spun to isolate platelets by centrifugation at 1,000 g for 10 minutes with prostacyclin (0.1 μg/mL) and ACD. The resulting pellet was suspended in Tyrode's buffer prepared fresh, and pre-warmed at 37°C (5 mM glucose, 1 mM $MgCl_2$, 20 mM HEPES, 12 mM $NaHCO_3$, 2.9 mM KCL, 0.34 mM Na_2HpO_4, 129 mM NaCl to a pH of 7.3). This suspension was spun again at 1,000 g with prostacyclin at the same concentration before being re-suspended to a final concentration of 2 x 10^8/mL. Platelets were left to rest for 30 minutes at room temperature before any further processing or treatment.

Platelet spreading.

Resting platelets were fixed by preparing platelets at a concentration of 4 x 10^7/mL and mixing with equal volumes of 10% neutral buffered Formalin in a 15 mL falcon tube. This mixture was inverted gently to mix the sample, and left to incubate for 5 minutes before subsequently adding 300 μL of the resulting fixed, resting platelets to coverslips coated in Poly-L-Lysine (Sigma). Cells were then spun down at 200 g for 10 minutes.

Spreading was performed on human fibrinogen (Plasminogen, von Willebrand Factor and Fibronectin depleted - Enzyme Research Laboratories) and Horm collagen (Takeda). Coverslips were coated overnight at a concentration of 100 μg and 10 μg/mL (fibrinogen and collagen) respectively, before blocking for 1 hour in denatured fatty acid free 1% BSA (Life Technologies). Finally coverslips were washed once with PBS before the addition of platelets. Unless otherwise stated (as in the time course experiment), platelets were spread for 45 minutes at 37°C. Fixation for spread platelets was performed in formalin as for resting platelets for 10 minutes.

Construct cloning and transfection.

β1-tubulin WT construct was generated by the gibson assembly (HiFi Kit, New England Biolabs) of a TubB1 sequence fragment synthesised as a gBlock by Integrated DNA Technologies (IDT) and a C-terminal mApple empty backbone (mApple-C1 was a gift from Michael Davidson (Addgene plasmid #54631; http://n2t.net/addgene:54631 ; RRID:Addgene_54631)[41]. All mutagenesis experiments were performed using the Q5 site directed mutagenesis kit from New England Biolabs following their supplied protocol. The table in supplementary figure S2 provides the primers and annealing temperatures used to produce the various mutants using the mAPPLE TubB1 plasmid as a template. All primers were designed using the online NEBase changer tool. Transfection was performed using a standard Lipofectamine 3000 protocol in Hek293T cells maintained in complete DMEM as described in the author's previous work[42,43].

Immunofluorescence.

After fixation platelets were washed twice with PBS before incubation in 0.1% Triton X-100 for 5 minutes. The subsequently permeabilised cells were washed twice with PBS before blocking in 2% Goat serum (Life Technologies) and 1% BSA (Sigma). Fixed, permeablised, and blocked cells were then incubated with primary antibodies at a concentration of 1:500 unless other-wise stated. The following antibodies were used for experiments in this work: polyglutamylated tubulin (mouse monoclonal antibody, clone B3 T9822, Sigma), pan-polyglycylated antibody (mouse monoclonal antibody, AXO49, MABS276 Millipore), monoglycylated antibody (AXO 962 mouse monoclonal MABS277, EMD Millipore), kinesin-1 (rabbit monoclonal to KIF1B ab 167429, abcam), axonemal dynein, β1-tubulin (Rabbit polyclonal PA5-16863), tyrosinated tubulin (rabbit monoclonal antibody, clone YL1/2, MAB1864, EMD Millipore), acetylated tubulin (Lys40, 6-11B-1, mouse monoclonal antibody, Cell Signalling Technology) and DNAI1 antibody (PA5-30643 Invitrogen).

After a 1 hour incubation in the relevant mix of primary antibodies. Cells were washed twice with PBS before incubation in secondary antibodies (Alexa-568-phalloidin, anti-rabbit Alexa-647, anti-mouse Alexa-588 (Life Technologies) for one hour at a dilution of 1:300 in PBS.

Stem Cell Culture.

Gibco human episomal induced pluripotent stem cell line was purchased from Thermo Scientific and cultured on Geltrex basement membrane in StemFlex medium (Thermo Scientific). Routine passaging was performed using EDTA (Sigma), with single cell seeding performed for transfection and attempted clonal isolation through the use of TrypLE (Thermo Scientific). Briefly, cells were washed twice with PBS and once with either EDTA (for clump passaging) or TrypLE (for single cell) before incubation in 1 mL relevant detachment media for 3 minutes at 37°C. For clump passaging, EDTA was removed and 1 mL of StemFlex added. Cells were detached by triturating media onto the bottom of the well and subsequently adding the required volume to fresh media (in a new, Geltrex coated plate). For single cell seeding, TrypLE was diluted in 2 mL StemFlex and the solution added to a 15 mL falcon tube for centrifugation at 200 g for 4 minutes. The supernatant was then discarded and the cell pellet resuspended in the required volume.

iPSC MK differentiation.

iPSC differentiation to mature, proplatelet forming megakaryocytes was performed using a protocol based on work published by Feng et al.[23]. To summarise, cells were detached by clump passaging and seeded on dishes coated with Collagen Type IV (Advanced Biomatrix) at 5 μg. Cells were seeded overnight with RevitaCell (Life Technologies) to support survival on the new basement substrate. To begin the protocol cells were washed twice and incubated in phase I medium comprised of APELII medium (Stem Cell Technologies) supplemented with BMP-4 (Thermo Scientific), FGF2-β, and VEGF (Stem Cell Technologies) at 50 ng/mL each. Cells were incubated at 5% oxygen for the first four days of the protocol before being placed in a standard cell culture incubator for a further two days in freshly made phase I medium. At day 6 of the protocol cells were incubated in phase II media comprised of APELII, TPO (25 ng/mL), SCF (25 ng/mL), Flt-3 (25 ng/mL), Interleukin-3 (10 ng/mL), Interleukin-6 (10 ng/mL) and Heparin (5 U/mL) (all supplied by Stem Cell Technologies). Each day in phase II media suspension cells were spun down at 400 g for 5 minutes and frozen in 10% FBS/DMSO. After 5 days of collection, all frozen cells were thawed for terminal differentiation. Terminal differentiation was performed by incubating cells in StemSpan II with heparin (5 U/mL) and Stem Cell Technologies Megakaryocyte Expansion supplement on low attachment dishes (Corning).

RNP Complexes.

The IDT Alt-R®RNP system was used to target and knock-out TUBB1. crRNAs were ordered at 2 nmol and resuspended in 20 μL TE buffer (IDT) for a final concentration of 100 μM. Atto-555 labelled tracrRNAs were ordered at 5 nmol and resuspended in a volume of 50 μL for a final concentration of 100 μM. To prepare small guide RNAs (sgRNA), equimolar ratios of both crRNA and tracrRNA were mixed with Nuclease Free Duplex Buffer (IDT). This mix was then incubated at 95˚C for 5 minutes before allowing the reaction mix to cool at -1˚C/second to 25˚C. This mix was then spun down and complexed with HiFi Cas9 V3 (1081058 - IDT) purified Alt-R®. Cas9 protein was diluted to 6 μg per transfection and incubated with an equal volume of annealed sgRNA. This mix was left for 30 minutes at room temperature to form complete and stable RNP complexes.

Stem Cell Transfection.

iPSC transfection was performed using Lipofectamine Stem (Life Technologies) according to manufacturer instructions. Briefly, iPSC were seeded on 24 well dishes coated with Geltrex at 50,000 cells per well. After an overnight incubation in StemFlex with RevitaCell, cells were washed twice with PBS and once with OptiMem before incubation in OptiMem with RevitaCell. RNP complexes were prepared as described in section and resuspended in 25 μL OptiMem per reaction. A Lipofectamine Stem master mix was prepared using 25 μL OptiMem and 2 μL Lipofectamine STEM per reaction (4 μL if a donor template is included). Equal volumes of both Lipofectamine and RNP mix were incubated to form lipofection complexes over a 10 minute incubation at room temperature. The final transfection mix was added to cells in OptiMem and left for 4 hours before the addition of StemFlex medium (and any relevant small molecules).

Measurement of iPSC transfection efficiency after treatment with Lipofectamine STEM and IDT RNP complexes was performed using manual cell counting in Evos acquired images (Phase contrast and fluorescence).

Microscopy.

Images were acquired using an Axio Observer 7 inverted epifluorescence microscope (Carl Zeiss) with Definite Focus 2 autofocus, 63x 1.4 NA oil immersion objective lens, Colibri 7 LED illumination source, Hammamatsu Flash 4 V2 sCMOS camera, Filter sets 38, 45HQ and 50 for Alexa488, Alexa568 and Alexa647 respectively and DIC optics. LED power and exposure time were chosen as appropriate for each set of samples but kept the same within each experiment. Using Zen 2.3 Pro software, five images were taken per replicate, either as individual planes (spread platelets) or representative Z-stacks (resting platelets). Images were prepared for presentation using Fiji (ImageJ). LUTs were adjusted for presentation purposes, and a rolling ball background subtraction applied. Where Z-stacks are taken, images are presented as a maximum intensity projection. Hek293T cells were imaged using an AiryScan confocal microscope as detailed in Smith et al.[44] dSTORM imaging of TTLL10 patient and control samples was performed as described by Khan et al.[42,43] applying dSTORM and ThunderSTORM reconstruction to samples labelled with AlexaFluor 647 in the presence of a blinking buffer.

Image analysis.

Image analysis of resting and spread platelets was performed using a customised workflow published by Pike et al[45]. Briefly, the actin channel from resting and spread platelet images was used to train Ilastik pixel classifiers (approximately 6 images per condition) for segmentation based on this channel as described by Pike et al.. This was incorporated into a KNIME workflow which would run images through the classifier to generated segmented binaries in which co-localisation and fluorescence intensity statistics were calculated[46–48]. For the data presented in this manuscript, $M1_{diff}$ (a corrected Mander's co-efficient to channel 1) was used to determine the co-localisation of PTMs to tubulin, and an $M2_{dif\ f}$ value (corrected Mander's co-efficient to channel 2) was used to calculate the co-localisation of motor proteins to PTMs of interest[49]. MKs and Hek293T were segmented manually by drawing a region of interest around cells in a projected Z-stack image. For co-localisation, these images were then fed through the same automated analysis pipeline as the platelet data[45] for co-localisation values. For measures of intensity in Hek293T images, cells were manually segmented (an ROI drawn) and fluorescence values in polyglutamylated and polyglycylated channels were subsequently measured and normalised to account for variation in transfection efficiency.

Quantitative Real Time PCR (qRT-PCR).

To determine whether the 13 mammalian TTLLs and 6 CCPs were expressed in iPSC-MKs at the different stages of differentiation (day 1, day 5 and day 5 +heparin) a qRT-PCR panel was developed using TaqMan technology and an ABI 7900 HT analyser (Applied Biosystems, Warrington, UK). RNA samples were isolated and reverse-transcribed and amplified with the relevant primers using SYBR-Green based technology (Power SYBR(r) Master Mix, Life Technologies). Total RNA was extracted from iPSC cells using the NucleoSpin RNA kit (Machery-

Nagel) and cDNA was synthesized using the High-Capacity cDNA Reverse Transcription Kit (Life Technologies). qRT-PCR was performed on all the TTLL/CCP fragments generated from primers designed in supplementary figure 5 and the housekeeping control GAPDH (GAPDHFOR 5'-GAAGGTGAAGGTCGGAGT-3' and GAPDHREV 5'-GAAGATGGTGATGGGATTTC-3'). Each reaction was set up in triplicate including a non-template control. Expression was analysed using the CT method using D1 undifferentiated cells as a control. A full list of primer sequences can be found in figure S8.

Supplementary Figures and Tables

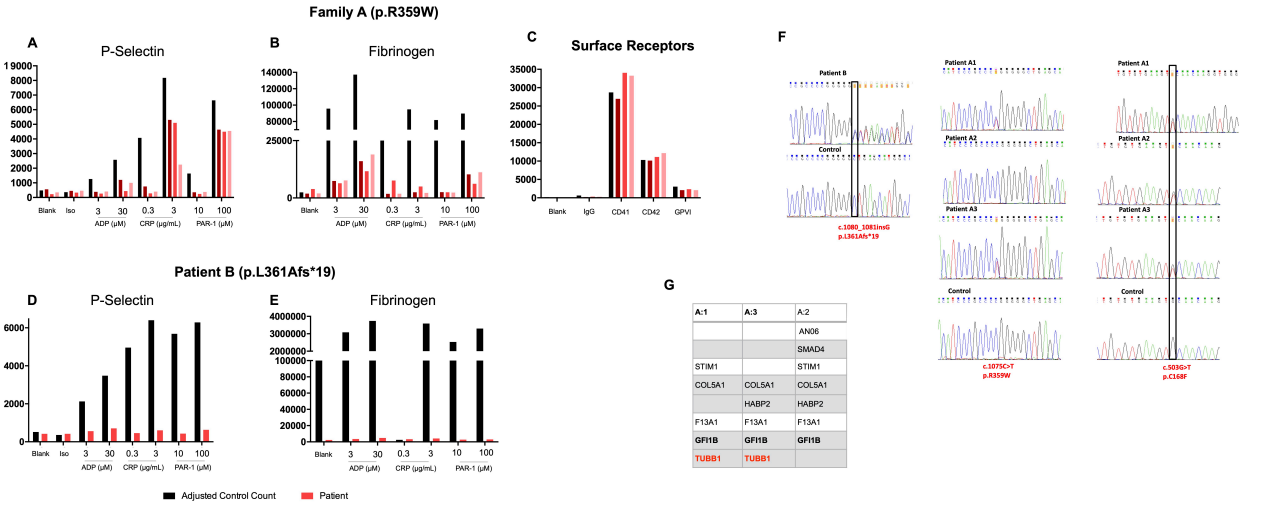

Fig. S1. Patient flow cytometry data reveals secondary defects. The GAPP project collects phenotypic data on patient recruitment, allowing for the assessment of secondary defects through FACS screening. (A) Individuals from family A show a reduction in P-selectin at both concentrations of CRP, and low concentration PAR-1. (B) Patients similarly show a reduction in fibrinogen uptake compared to controls, but show no difference in (C) surface marker expression. (D) Patient B shows a marked reduction in P-selectin surface expression and (E) fibrinogen uptake compared to controls. Platelet surface receptor normal range values (from healthy volunteers) - Blank –190 (SD 27); isotype control - 637 (SD 208); CD41 – 28727 (15378); CD42b – 10318 (SD 4257); GPVI – 5693 (SD 2447). P-selectin mean responses (Neat PRP) : Blank – 485 (SD 132); ADP 3 µm – 1261 (SD 558); ADP 30 µm – 2575 (SD 742). CRP 0.3 µg/mL– 4076 (SD 2297); CRP 3.0 µg/mL – 8177 (SD 1781). PAR-1 10 µM – 1636 (SD 1118); PAR-1 100 µM – 6642 (SD 1211). Fibrinogen mean responses (Neat PRP) : Blank – 2442 (SD 1253); ADP 3 µm – 95756 (SD 57434); ADP 30 µm – 137242 (SD 99347). CRP 0.3 µg/mL– 35095 (SD 62454); CRP 3.0 µg/mL – 94905 (SD 63054). PAR-1 10 µM – 81794 (SD 75990); PAR-1 100 µM – 89744 (SD 54673). (F) Sanger sequencing of patient samples from Family A. (G) WES analysis and subsequent genetic variant interpretation in Family A. This was performed using the clinical variant interpretation platform Congenica https://www.congenica.com) and candidate genes were filtered and selected based on an Inherited bleed-ing Disorder (IBD)-specific panel of 119 genes[29]. The following rare variants were found collectively within the different individuals of family A (AN06 - ENST00000435642.1:c.1165+21delT, COL5A1 - NM_000093.4:c.4760T>G, NP_000084.3:p.Ile1587Ser, F13A1 - NM_000129.3:c.-18-7dupT, GFI1B - NM_004188.4:c.503G>T, NP_004179.3:p.Cys168Phe, HABP2 - NM_004132.3:c.1046G>A, NP_004123.1:p.Gly349Glu, TUBB1 - NM_030773.3:c.1075C>T, NP_110400.1:p.Arg359Trp, SMAD4 - NM_005359.5:c.-127-1G>T, STIM1 - NM_003156.3:c.974G>A, NP_003147.2:p.Arg325Gln). Individuals and their variants with a low platelet count are shown in red font where only GFI1B and TUBB1 variants are common to both individuals.(H) Clinical and laboratory interpretation of the GFI1B and TUBB1 variants found in individuals of family A. In silico prediction tools tools used were as follows (POLYPHEN http://genetics.bwh.harvard.edu/pph2/; SIFT https://sift.bii.a-star.edu.sg; Align GVGD http://agvgd.hci.utah.edu/agvgd_input.php). Population frequencies were obtained from the genome aggregation database (Gnomad https://gnomad.broadinstitute.org). Current ACMG guidelines are used as supporting evidence; PP1: co-segregation with disease in multiple affected family members in a gene definitively known to cause the disease; PP3: Multiple lines of computational evidence support a deleterious effect on the gene or gene product (conservation, evolutionary, splicing impact, etc.)

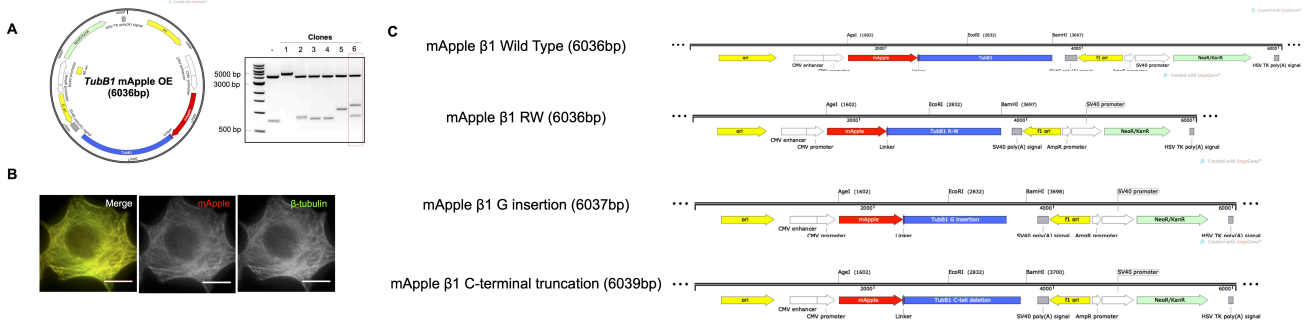

D

	Primers	Annealing temperatures (°C)
RW	F: 5' CATCCCGCCCtGGGGGCTGAG 3' R: 5' TCGCAGACAGCCACCTTGACG 3'	72
G insertion	F: 5' GCTGAGCATGGCCGCCACCTTC 3' R: 5' CCCCCGGGGCGGGATGTC 3'	72
C tail truncation	F: 5' TAAGAGGAAGATGAAGAGGTC 3' R: 5' TAGAACTGCTTTGGCATC 3'	59

Fig. S2. Generation of WT and mutated mApple-β1-tubulin plasmids. (A) An N-terminal mApple-β1 tubulin over expression vector was designed and cloned through the gibson assembly of the β1 tubulin sequence into a C-terminal mApple construct (mApple-C1 was a gift from Michael Davidson (Addgene plasmid # 54631 ; http://n2t.net/addgene:54631 ; RRID:Addgene_54631). Of the 6 selected clones presented, clone 6 demonstrated cleavage bands of the predicted molecular weight, and was subsequently cloned. (B) The correctly assembled sequence was then transfected to and co-stained with a β-tubulin antibody to confirm the correct expression and fold of this tubulin construct. (C) Mutants of the WT construct were generated through a Q5 site directed mutagenesis kit to generate constructs harbouring patient RW and G insertion mutants, as well as an artificially designed C-terminus truncation of the protein. (D) Primers used for the site directed mutagenesis are listed with their respective annealing temperatures.

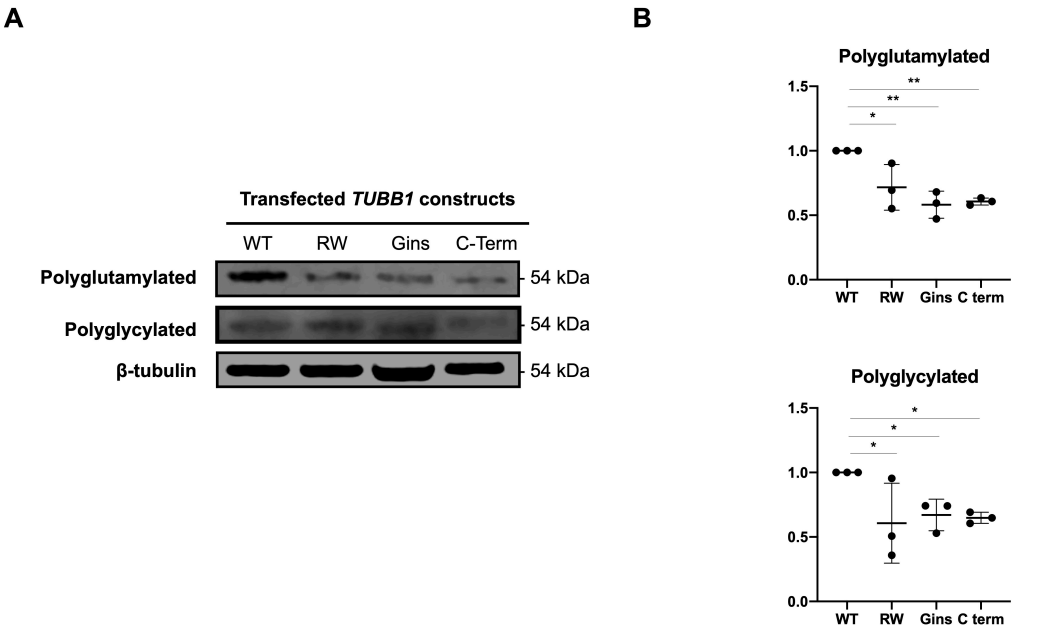

Fig. S3. Western blotting of TubB1 mutant constructs. Mutant TubB1 constructs were re-cloned without the mApple label and transfected into Hek293T. Transfected cells were then collected and lysed for western blotting. (A) A reduction in polyglutamylation and polyglycylation is evident when compared to wild type TubB1 constructs. (B) Polyglutamylation was significantly reduced in RW, G insert, and C terminal truncations (* p = 0.0102, ** p = 0.0011, ** p = 0.0017), as was polyglycylation (* p = 0.0210, 0.0434, p = 0.0338.).

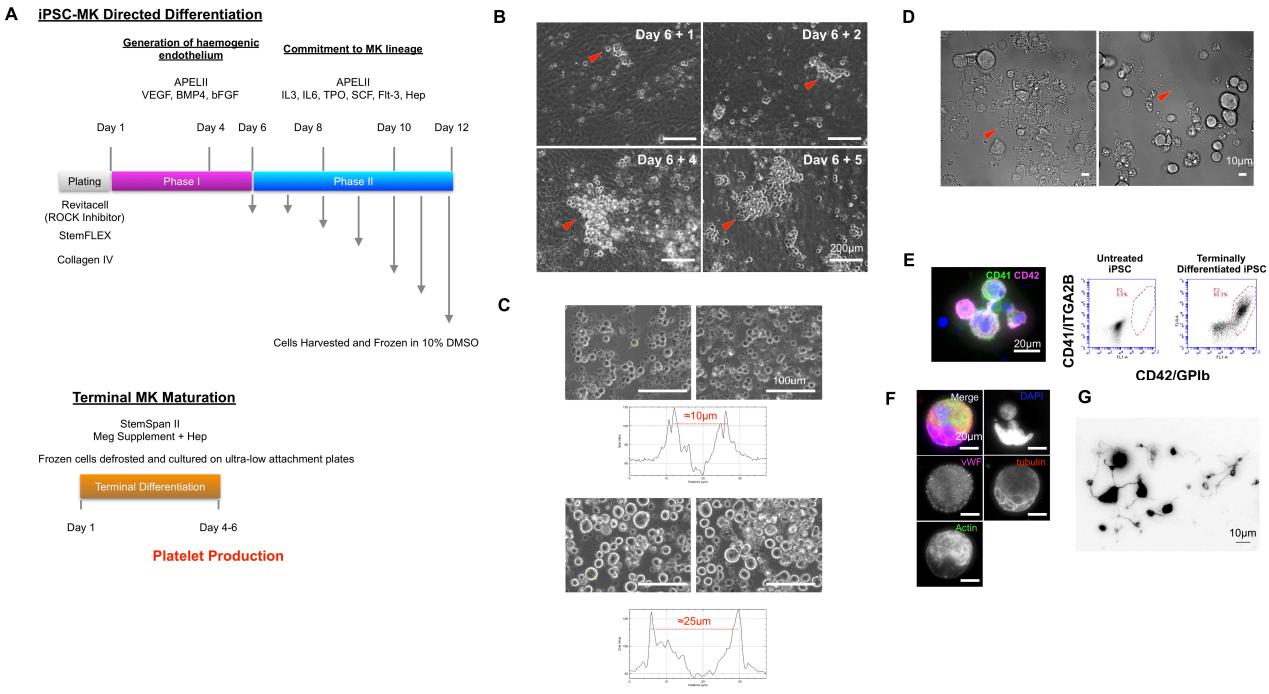

Fig. S4. Directed differentiation of iPSC to proplatelet forming MKs. (A) A 3 stage protocol was adapted from a method previously published by Feng *et al.*. Briefly, iPSC were clump passaged on to collagen IV coated plates and incubated in RevitaCell overnight before beginning Phase I of the differentiation. Phase I involves a 4 day incubation at 5% O_2 in APEL2 media supplemented with 50ng of BMP4, VEGF, and FGF2, after which fresh media was added and cells were incubated for 2 more days at normoxic conditions. Phase II of the protocol involved incubation in APEL2 supplemented with IL3, IL6, Flt-3, hSCF, TPO, heparin, during which time cells were harvested and frozen every 48 hours and fresh media added. Finally, harvested cells were thawed and incubated in StemSpan II medium with MK supplement for 5 days before samples were prepared for downstream assays (immunofluorescence, RT-PCR etc.). (B) During Phase II of the differentiation, progressively larger numbers of blast like cells are observed emerging from a layer of haemogenic endothelium. (C) During Phase III of the differentiation, cells grow from progenitors and blast like cells approximately 10 μm in size to large, mature MKs ranging in 25-40 μm in size. (D) At day 5, on treatment with Y-27632 and heparin, cells form elaborate proplatelet networks. (E) 60% of terminally (Phase III) differentiated cells are CD41 and CD42 double positive and on staining demonstrate (F,G) a mix of ploidies and proplatelet networks consistent with mature platelet producing MKs.

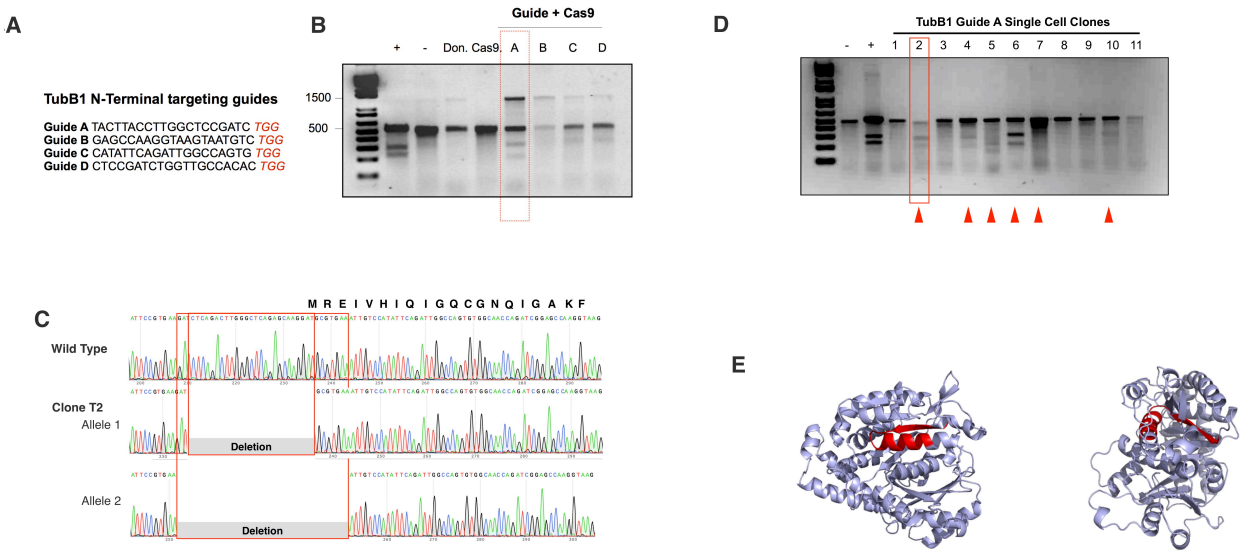

Fig. S5. CRISPR bi-allelic knock-out of β1 tubulin. (A) Guides targeting exon 1 of the *TUBB1* gene were designed and (B) tested for efficiency using a T7EI cleavage assay. The population evidencing the most cleavage (and hence most efficient guide (guide A)) was taken forward to generate *TUBB1* knock-out clones, through single cell clonal isolation. (C) Cells positive for cleavage on single cell expansion (identified by the red arrows) were taken forward for sequencing. (D) Clone T2 revealed a bi allelic loss of the start codon, (E) resuling in a deletion of a significant portion of the N-terminus and as evidenced in the main text, a loss of *TUBB1* expression.

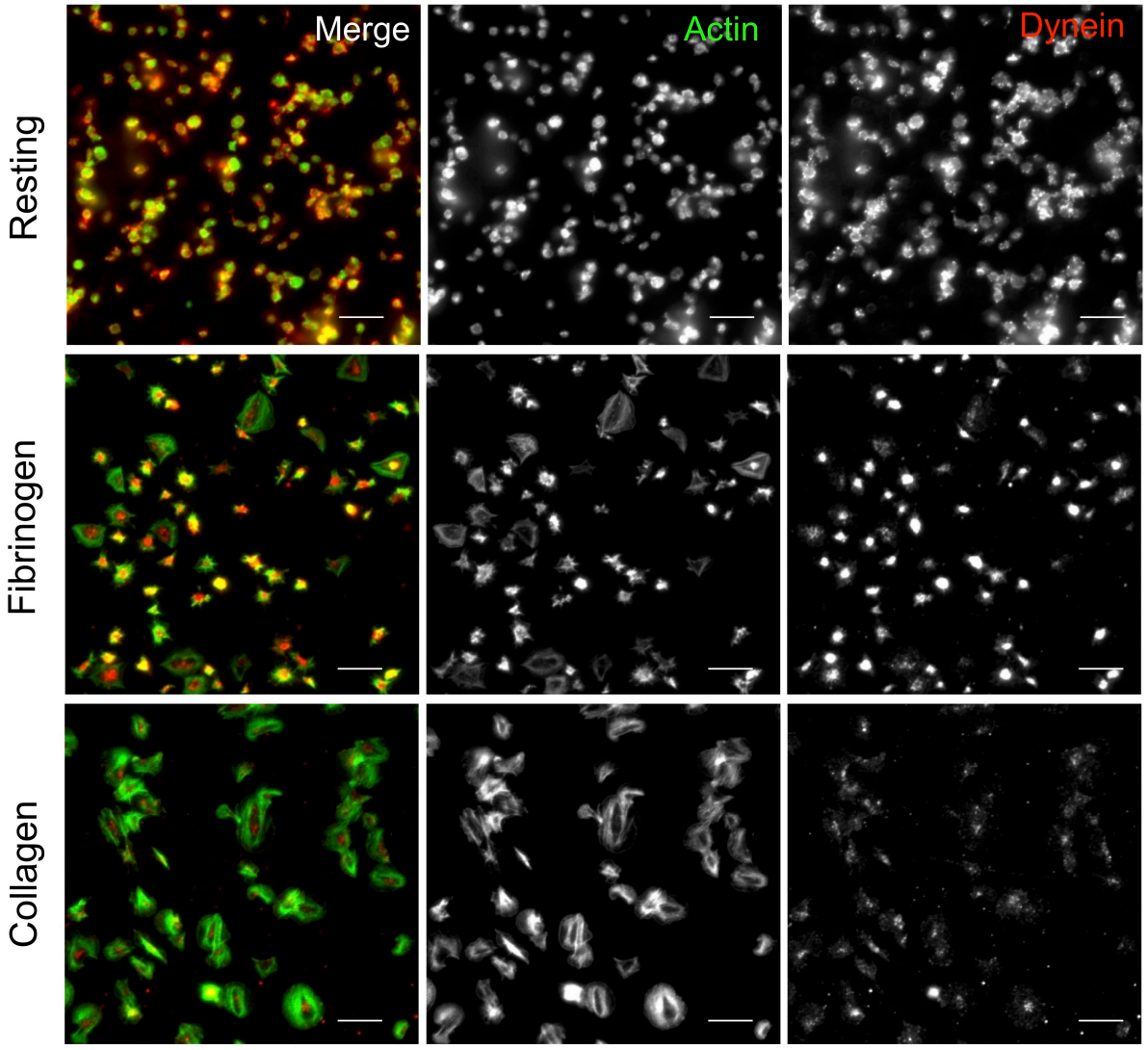

Fig. S6. Staining of Cytoplasmic Dynein in resting and Spread Platelets. Resting and spread human donor platelets were stained for cytoplasmic dynein to compare the distribution of this isoform of the motor protein to axonemal dynein. While axonemal dynein is primarily found on the edge of spreading cells, cytoplasmic dynein is found at the centre of spread cells, suggesting that the axonemal variant is involved in platelet spreading and activation.

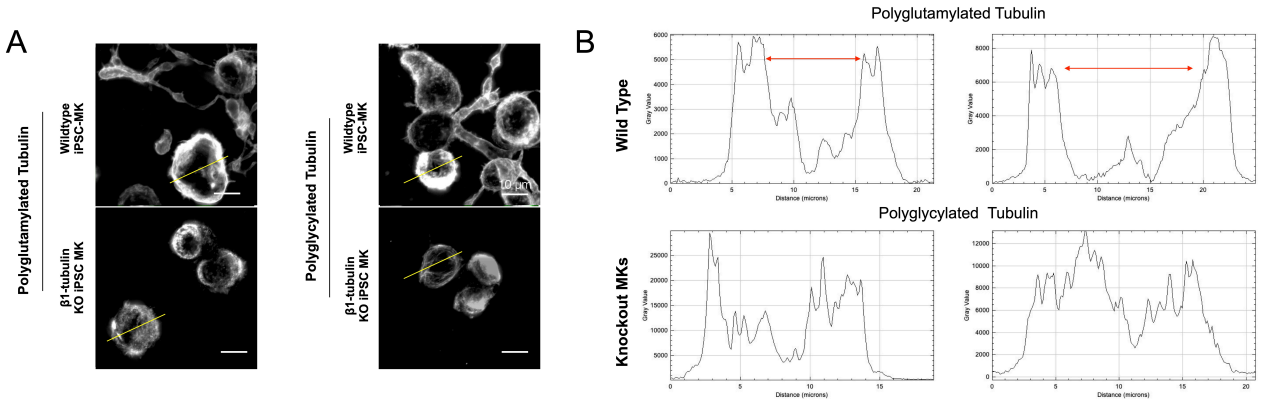

Fig. S7. Line profiles demonstrating difference in distribution of polymodified tubulin in knock-out cells. Line profiles demonstrating the different distribution of polymodified residues in wild type vs. knock-out iPSC MK. In wild type cells, both polymodifications accumulate around the periphery of mature cells forming a dense microtubule band indicated by distinctive peaks on their respective line profiles (B). In contrast, knock-out cells have a disordered and diffuse distribution of tubulin indicated by their line profiles.

Name	Sequence : (5' to 3')	Fragment Size	Name	Sequence : (5' to 3')	Fragment Size
FH1_TTLL1	AGTCAACCATTTTCCAAACC	143 bp	FH1_TTLL11	ATTTGTTTATCCGGTTCCTG	76 bp
RH1_TTLL1	AGTCCAGATAGAGGTATTTTCC		RH1_TTLL11	CTCCTTATGAAGGTACGAAAG	
FH1_TTLL2	GCCTTTACCCTTAACATTCC	138 bp	FH1_TTLL12	CATTCTGGAGGAAAACAAGG	84 bp
RH1_TTLL2	TTTCTTCTTCTCCAGTGTTG		RH1_TTLL12	GTGTAGACCTTGAAGATGTG	
FH1_TTLL3	AAGCCTTCATAGAGGACTTC	95 bp	FH1_TTLL13	ACCTGACCAACTATGCTATC	477 bp
RH1_TTLL3	TACTGCCTGAATAGGGTATG		RH1_TTLL13	TGGTTTTGATGATGATGTCC	
FH1_TTLL4	GAAGCTAAACCATTTCCCAG	106 bp	FH1_AGTPBP1 (CCP1)	AAAAACAAATGCCAGGAGAG	100 bp
RH1_TTLL4	GAAACTGAACTCCTTCTTGC		FH1_AGTPBP1 (CCP1)	CATGTTTCTATGCCGGTTATC	
FH1_TTLL5	AATTCATATTCGAAGGACCG	85 bp	FH1_AGBL2 (CCP2)	GGCCTATCAGTTTATCTTCAG	170 bp
RH1_TTLL5	GATTGTTGATCAGGTAGACG		RH1_AGBL2 (CCP2)	ATCTGTAATCCCAGCTACTC	
FH1_TTLL6	AAGCCCTTTATCATTGATGG	87 bp	FH1_AGBL3 (CCP3)	GAAGAGCAAAGAAGGAACAG	102 bp
RH1_TTLL6	GTACACAAAAATCCTGAGAGG		RH1_AGBL3 (CCP3)	TTGTTACCCAGAGTAGATCC	
FH1_TTLL7	CAGAATTGGTGGTAAAGACC	152 bp	FH1_AGBL1 (CCP4)	AGATGATGACTTGGAAACAG	111 bp
RH1_TTLL7	CCATGGCTTTAGTTTTCTATCC		RH1_AGBL1 (CCP4)	CTATAGGAGAGCTCAAGACAC	
FH1_TTLL8	AACAAGGAATTTCCCAAGAC	174 bp	FH1_AGBL5 (CCP5)	CTATATCCAAAGCTCATCTCC	178 bp
RH1_TTLL8	AGTGGAACTTCTTCTCTACC		RH1_AGBL5 (CCP5)	AGTTGCATTCAAGTGTGTAG	
FH1_TTLL9	ATCATGAAGCCTGTAGCC	158 bp	FH1_AGBL4 (CCP6)	AAATGATGATGCCATTGGAG	114 bp
RH1_TTLL9	GGATTTTCAATGTAACGCTG		RH1_AGBL4 (CCP6)	TTACCACTTTCAAAGCAAGC	
FH1_TTLL10	GAAGAGTTTTTCCCAGAGAC	90 bp			
RH1_TTLL10	GATCCATATCTGGGTTTCATC				

Fig. S8. Primers and predicted fragment lengths for qRT-PCR screen of TTLL and CCP expression. Exon overlapping primers were disgned for a qRT-PCR screen of TTLL and CCP expression. Forward and reverse primer sequences are listed, along with predicted fragment length.

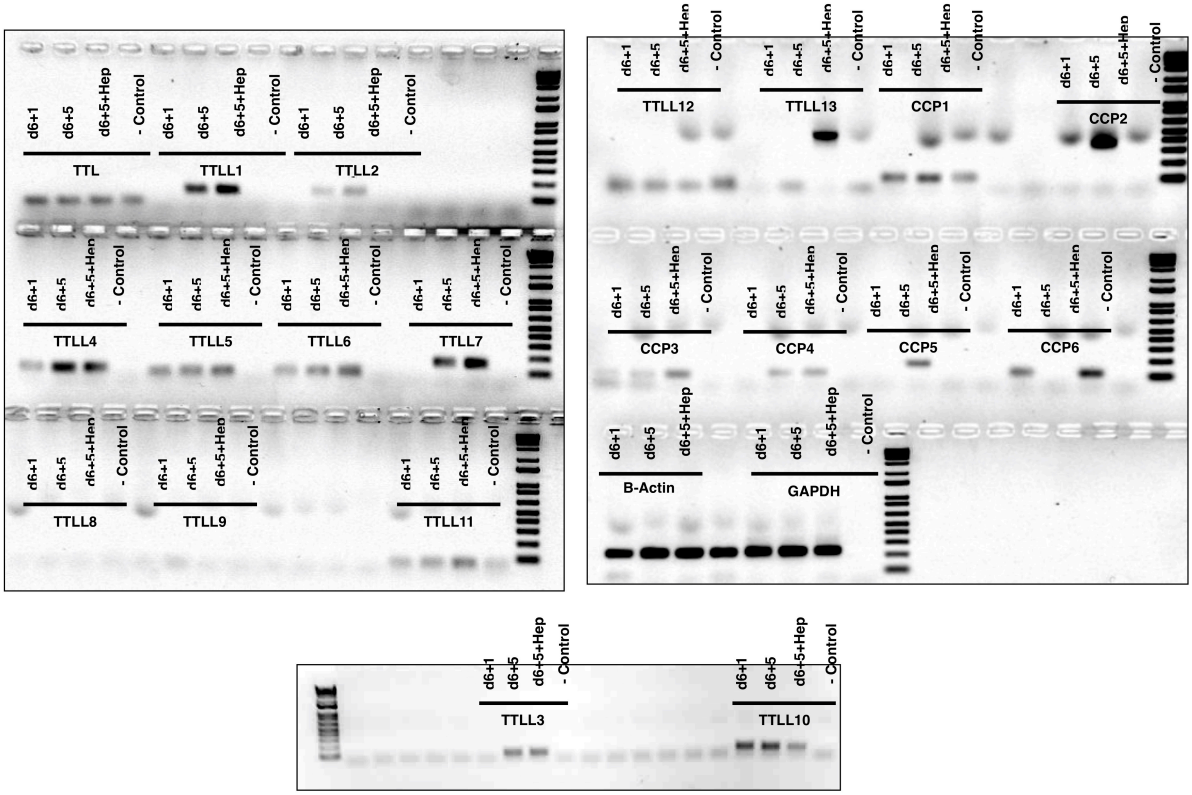

Fig. S9. Whole gel for TTLL and CCP RT-PCR screen in iPSC-MKs. Complete gels used in figure 6.

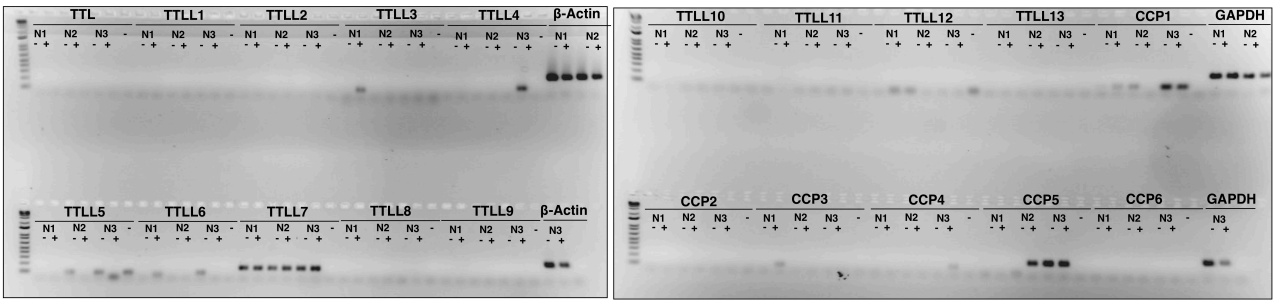

Fig. S10. Whole gel for TTLL10 and CCP RT-PCR screen in human peripheral blood platelets. Complete platelet gel used in figure 6.

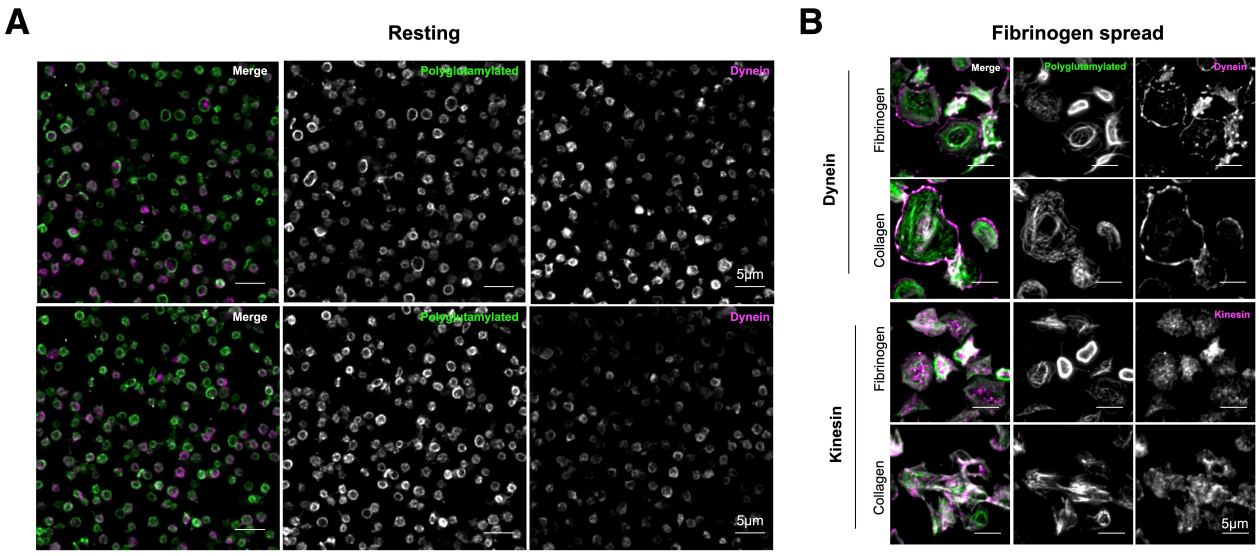

Fig. S11. Resting platelets co-stained for dynein and kinesin. Resting platelets co-stained for kinesin and dynein to supplement spread figures.

	Family A		Family B	
	II:2	II:3	II:2	III:1
Total number of variants identified by WES	26,302	26,379	26,456	27,018
Total number of variants (excluding synonymous) with a MAF ≤ 0.01	2,282	2,277	2,378	2,601
Shared significant variants from the panel of platelet and endothelial cell genes with a MAF ≤ 0.01	11		11	
Total number of novel variants	159	167	129	140
Total number of shared novel variants	51		53	
Total number of shared genes predicted to be pathogenic using all bioinformatics tools	9		11	

Family A, II:2 & II:3							
Gene	**Genomic variation**	**Protein effect**	**Variation type**	**Prevalence**	**Mutation taster**	**ACMG criteria**	**Classification**
TTLL10	c.462delG	p.P154Rfs*38	Frameshift deletion	Novel	Disease causing	PM2 PP3 PM4	Uncertain significance
Family B, II:2 & III:1							
Gene	**Genomic variation**	**Protein effect**	**Variation type**	**Prevalence**	**Mutation taster**	**ACMG criteria**	**Classification**
TTLL10	c.745_746insG	p.V249Gfs*57	Frameshift insertion	2.15×10^{-3}	Disease causing	PM2 PP3 PM4	Uncertain significance

Fig. S12. Rare and novel TTLL10 genetic variants identified in WES data from affected individuals. Variants were filtered; synonymous variants and variants with a minor allele frequency (MAF) were excluded, and non-shared variants. The pathogenicity of the remaining variants was predicted using tools (Mutation Taster, Phastcons, SIFT, Provean etc.) and American College of Medical Genetics and Genomics (ACMG) classification Candidate variants are selected on the basis of a pathogenic prediction. Supporting evidence is given where PM2 is “Absent from controls (or at extremely low frequency if recessive) in Exome Sequencing Project, 1000 Genomes Project, or Exome Aggregation Consortium”, PP3 is “Multiple lines of computational evidence support a deleterious effect on the gene or gene product (conservation, evolutionary, splicing impact, etc.)” and PM4 is “Protein length changes as a result of in-frame deletions/insertions in a non-repeat region or stop-loss variants”.

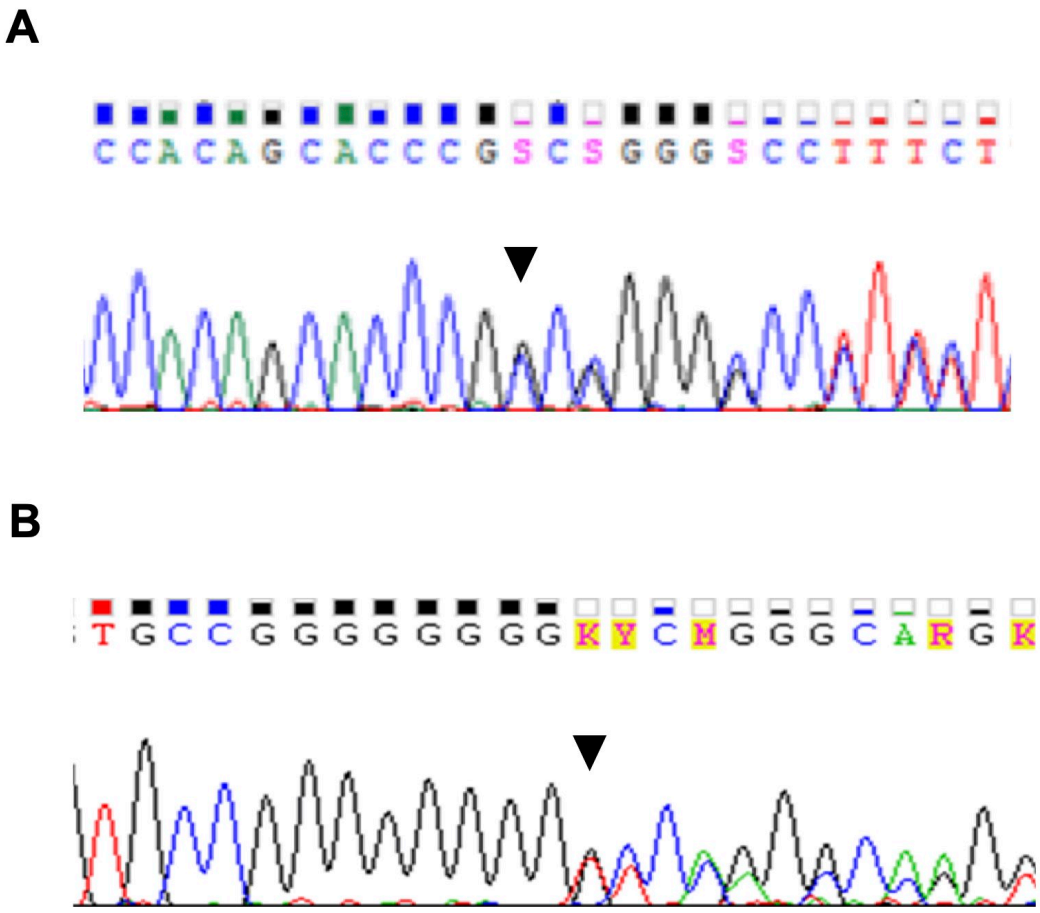

Fig. S13. Supplementary figure 13 Sanger sequencing of the TTLL10 variants for confirmation following WES. Representative confirmative Sanger sequencing electropherograms are shown. Black arrow shows sites of genomic variation. A) c.462delG. B) c.745_746insG. Reference sequence- NM_001130045.